Aeolian Research 15 (2014) 53–71

Contents lists available at ScienceDirect

Aeolian Research

journal homepage: www.elsevier.com/locate/aeolia

The size distribution of desert dust aerosols and its impact on the Earth system

Natalie Mahowald [a,*], Samuel Albani [a], Jasper F. Kok [a,b], Sebastian Engelstaeder [c], Rachel Scanza [a], Daniel S. Ward [a], Mark G. Flanner [d]

[a] Department of Earth and Atmospheric Sciences, Cornell University, Ithaca, NY 14853, United States
[b] Department of Atmospheric and Oceanic Sciences, University of California, Los Angeles, CA 90095, United States
[c] School of Geography and the Environment, University of Oxford, South Parks Road, Oxford OX1 3QY, UK
[d] Department of Atmospheric, Oceanic and Space Sciences, University of Michigan, Ann Arbor, MI 48105, United States

ARTICLE INFO

Article history:
Available online 18 November 2013

Keywords:
Desert dust
Size distribution
Biogeochemistry
Radiative effects
Indirect effects on clouds

ABSTRACT

The global cycle of desert dust aerosols responds strongly to climate and human perturbations, and, in turn, impacts climate and biogeochemistry. Here we focus on desert dust size distributions, how these are characterized, emitted from the surface, evolve in the atmosphere, and impact climate and biogeochemistry. Observations, theory and global model results are synthesized to highlight the evolution and impact of dust sizes. Individual particles sizes are, to a large extent, set by the soil properties and the mobilization process. The lifetime of different particle sizes controls the evolution of the size distribution as the particles move downwind, as larger particles fall out more quickly. The dust size distribution strongly controls the radiative impact of the aerosols, as well as their interactions with clouds. The size of particles controls how far downwind they travel, and thus their ability to impact biogeochemistry downwind of the source region.

1. Introduction

Mineral aerosols or desert dust particles are soil particles suspended in the atmosphere in regions with easily erodible dry soils, little vegetation and strong winds. Mineral aerosols represent one of the most important aerosols in mass and aerosol optical depth (Tegen et al., 1997), and can significantly impact radiation during strong events or even in the annual mean (Li et al., 2004). Desert dust can interact with liquid or ice clouds, and thereby modify cloud optical properties and lifetimes (DeMott et al., 2003; Mahowald and Kiehl, 2003), as well as affect precipitation processes (Creamean et al., 2013). Once dust particles are deposited to the surface, they provide micro nutrients to the ocean (e.g. Jickells et al., 2005; Martin et al., 1991) or to land ecosystems (e.g. Okin et al., 2008; Swap et al., 1992), as well as modify snow albedo (Painter et al., 2007). Furthermore, inhalation of dust aerosol poses a hazard to human health. The smaller the aerosol, the greater the chance of it getting deposited in the gas-exchange region of the lungs, and the greater the adverse effect (e.g., Brunekreef and Holgate (2002)). Thus mineral aerosols are important for human health, weather, climate, and biogeochemistry (Fig. 1).

Soil dust particles are entrained into the atmosphere in a several step process (e.g. Marticorena and Bergametti, 1995; Kok et al., 2012). First strong winds force particles of about 100–200 μm diameter to move in ballistic trajectories ('saltation') close to the surface (Bagnold, 1941; Alfaro et al., 1998b). These saltating particles can break apart or eject smaller soil particles upon impacting the soil. These smaller particles (< ~50 μm) are entrained into the boundary layer, after which they can be transported long distances (Prospero, 1996; Grousset et al., 2003).

Mineral aerosols are highly variable in space and time, with variability in mass of more than 4 orders of magnitude (e.g. Mahowald et al., 2009). Much of the desert dust mass transported in the atmosphere occurs during a few events (e.g. Mahowald et al., 2009). Globally averaged mineral aerosols have varied by a factor of 2–3 between glacial and interglacial time periods (Mahowald et al., 2006; Petit et al., 1999), and on the regional and decadal time scale can change by a factor of 2–4 depending on climate or land use by humans (Ginoux et al., 2012; Mahowald et al., 2010; Prospero and Lamb, 2003).

For aerosols, chemical composition and size are critical in considering the impacts (e.g. Mahowald et al., 2011a,b). For mineral aerosols, both composition and size vary greatly over space and time. Here we focus on size. The lifetime of a particle is heavily dependent on the size of the particle, because smaller particles fall

* Corresponding author. Tel.: +1 607 255 5166.
E-mail address: mahowald@cornell.edu (N. Mahowald).

http://dx.doi.org/10.1016/j.aeolia.2013.09.002
1875-9637/

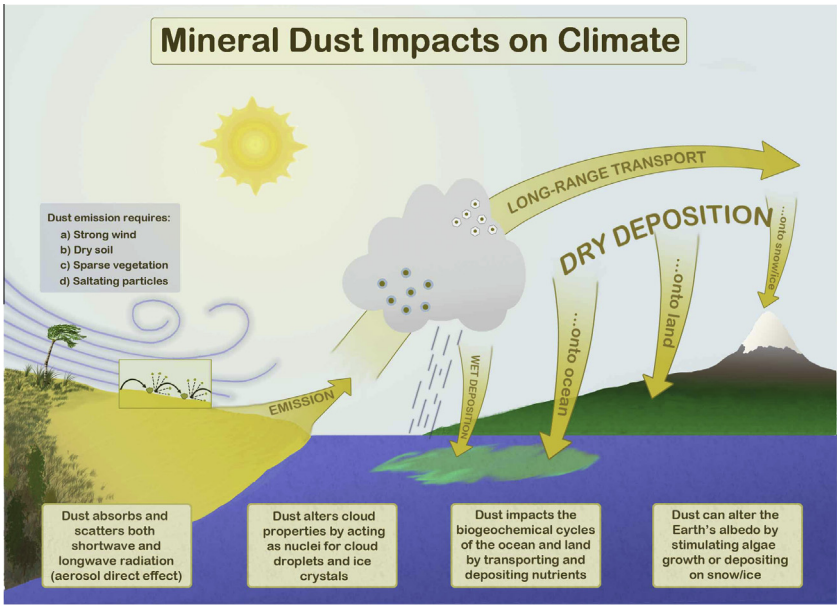

Fig. 1. Schematic of interactions between dust and climate and biogeochemistry.

downward much slower than larger particles because of friction (Seinfeld and Pandis, 1998). For instance, recent results from the Fennec field campaign in the Sahara desert indicate that the lifetime of dust aerosols larger than 20 μm is of the order of 12 h (Ryder et al., 2013a). For impacts through direct solar radiation interactions, particles with sizes of the order of the solar (shortwave) wavelengths (~0.2–2 μm) produce the largest shortwave (generally cooling) radiative effect per unit mass. Conversely, particles with sizes of the order of terrestrial (longwave) radiation (> ~4 μm), produce the largest longwave (warming) radiative effect (Miller et al., 2006; Tegen and Lacis, 1996). For indirect effects with clouds, although larger particles become cloud condensation nuclei first, the number of particles activated in a cloud is important, and thus the number of particles above a given size is the important quantity (Dusek et al., 2006). For biogeochemical impacts, the amount of mass deposited is important, and thus large particles can dominate. Thus, size is a key determinant of mineral aerosol impacts. However, the size distribution of dust is poorly understood and difficult to consistently measure (e.g. Reid et al., 2003b).

There have been several recent reviews of desert dust impacts on climate and biogeochemistry (e.g. Jickells et al., 2005; Mahowald et al., 2005; Shao et al., 2011b), although none have focused on dust sizes. For this review, we focus on the characterization and spatial patterns of the size distribution, and describe how size impacts mineral aerosol impacts on climate and biogeochemistry. In Section 2 we review methods for characterizing dust particle distributions in both observations and models. Section 3 focuses on the distribution of dust particle sizes, and Section 4 on the importance of size for the impacts of dust onto climate and biogeochemistry. Section 5 summarizes the results and identifies key areas for more research.

2. Method for measuring and modeling the dust particle size distribution

2.1. Dust size distributions

Aerosols can vary in size from less than 1 nm up to 100 μm. Aerosols less than 1 μm are considered fine aerosols, and are divided into Aitken mode (<0.1 μm) and accumulation model (>0.1 μm). Particles larger than about 1 μm are often referred to as coarse particles. The size distribution of aerosols is often found to be a log-normal distribution (Fig. 2), (although not necessarily close to the source regions, as discussed later). The important properties of aerosols, which are related to the size distribution, include the number, surface area and the mass of particles (Fig. 2). Assuming there is a simple log-normal distribution, there is a straightforward mathematical relationship between number, surface area and mass (e.g. Seinfeld and Pandis, 1998).

The particle size can be characterized using different particle properties, resulting in a range of measures of the particle diameter, including the aerodynamic, geometric, and optical diameters. Since dust aerosols can be highly irregular, especially if they are aggregates (Okada et al., 2001; Reid et al., 2003a), these different measures of particle size can differ strongly for the same particle (Reid et al., 2003b).

Most studies discussing particle size concern themselves with the *geometric diameter* D_p, which is defined as the diameter of a sphere having the same volume as the irregularly-shaped dust particle (e.g., Hinds, 1999). This diameter can be measured using a variety of experimental techniques (see Table 1), including through use of a *coulter counter* (see Table 1), which infers the particle volume by measuring the changes in electrical resistance as the particle flows in an electrolyte suspension through a narrow orifice (Hinds, 1999). The geometric diameter can also be determined using imaging techniques, such as optical microscopy (e.g., Gillette et al., 1972) and electron microscopy (e.g. Reid et al., 2003a). A disadvantage of imaging techniques is that only two of the three particle dimensions can normally be measured, although the third dimension can be estimated using shadowing techniques (Okada et al., 2001).

Whereas the geometric diameter is based on the particle's physical size, the *aerodynamic diameter* D_{ae} is determined by the particle's aerodynamic resistance. It is defined as the diameter of a spherical particle with density $\rho_0 = 1000\ kg/m^3$ that has the same aerodynamic resistance as the dust aerosol. The aerodynamic diameter is of critical importance in assessing the health impacts of mineral dust and other aerosols, since it determines where in the human body aerosols are deposited upon inhalation (e.g., (Brunekreef and Holgate, 2002)). Consequently, the aerodynamic diameter is commonly used in setting air pollution standards, such as limits in Europe and the United States on concentrations of

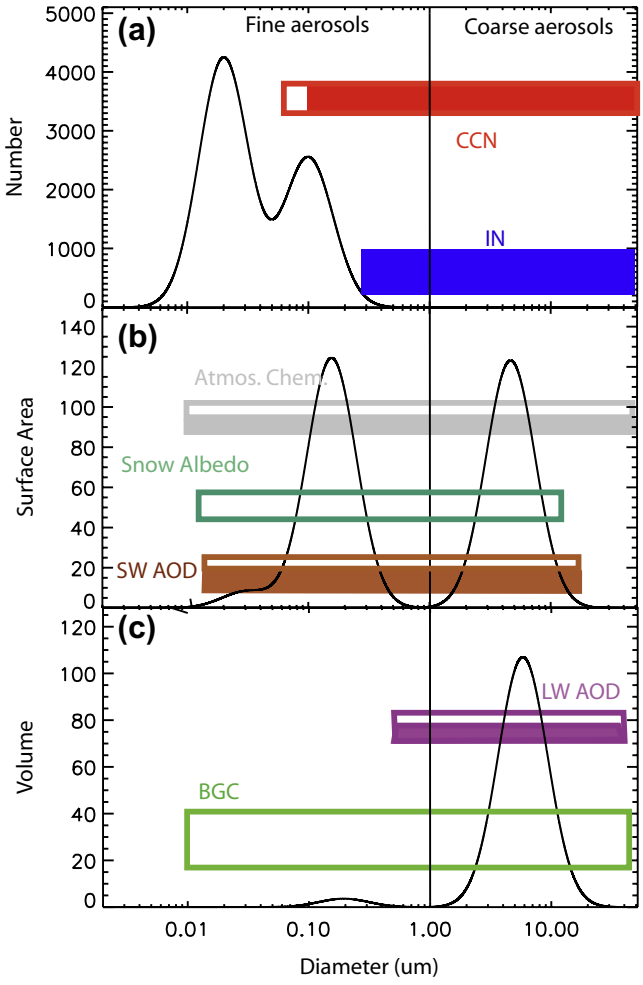

Fig. 2. (a) Aerosol number, (b) surface area, and (c) volume for a typical trimodal aerosol distribution (from (Mahowald et al., 2011a,b)) based on information in figure 7.6 in (Seinfeld and Pandis, 1998) and on information in (Dulac et al., 1996). Also shown in the boxes is a schematic representation of the typical aerosol diameter range impacting various processes as described in the text. Each process is assigned a panel depending on whether the impacts are primarily dependent on number (CCN and IN), surface area (SW AOD and LW AOD) or mass (biogeochemistry). Abbreviations: CCN, cloud condensation nuclei (*red*); IN, ice nuclei (*blue*); SW AOD, shortwave aerosol optical depth (*brown*); LW AOD, longwave aerosol optical depth (*purple*); and BGC, biogeochemically relevant species (*green*). Solid boxes represent only size-dependent processes, and the outlined boxes represent the part of the impact that is composition dependent.

PM2.5 and PM10 (i.e., particles with aerodynamic diameters smaller than 2.5 and 10 μm, respectively) (Hinds, 1999). The aerodynamic diameter can for instance be measured with a cascade impactor (see Table 2), which uses differences in particle inertia to deposit particles of decreasing aerodynamic diameter on a sequence of stages (Hinds, 1999). The geometric and aerodynamic diameters can be mathematically related (e.g., Reid et al., 2003b).

Lastly, the *optical diameter* D_{op} is defined by the particle's optical scattering abilities, (often defined as the radaius of a sphere with the same surface area) and is usually measured using optical sizing instruments such as the Malvern multisizer. These instruments measure the intensity of scattered light at different values of the angle with the incident beam, and then use knowledge of the particle's index of refraction to convert this measurement into an estimate of particle size (Hinds, 1999). Related to the optical diameter is the use of optical inversion techniques of remote sensing data, such as used by the AErosol RObotic NETwork (AERONET). These products use retrieval models to obtain the columnar volume size distribution that best fits measurements of spectral and multiangle sun-sky radiances (Dubovik and King, 2000).

Unless otherwise noted, references to particle size in the remainder of this article refer to the geometric diameter.

2.2. Dust size distribution: observational methodologies

A complete understanding of the dust cycle requires knowledge of processes related to dust emissions and the spatial evolution of dust load and its size distribution with transport and deposition. This ranges from saltating particles, to loess deposits often representative of proximal sedimentation, to remote sites such as ice cores preserving information representative of long range transport (Maher et al., 2010). Observations providing information of dust size distributions can be obtained from aeolian sediments, *in situ* sampling and remote sensing. The time and space represented in the measurement as well as the quantity measured varies depending on the kind of measuring device (Table 1; see also Section 2.1). Measurement accuracy and precision are limited by the signal-to-noise issue when attempting to isolate the dust (signal) from the surrounding environment or physical matrix.

Aeolian sediments include paleodust records (Kohfeld and Harrison, 2001; Maher et al., 2010), embracing a broad spatial range of distance from the dust sources, including the more traditional loess/paleosols sequences (e.g. Pye, 1995), marine sediments (e.g. Rea, 1994) and ice cores (e.g. Petit et al., 1999), and the more recent developing dust records from lacustrine sediments (e.g. Lim and Matsumoto, 2008) and peat bogs (e.g. Marx et al., 2009). In the case of sediments the general procedure is to apply mechanical, chemical and thermal processes to isolate the terrigenous fraction from the sediment, after which the sample is put into water and a dispersant is added to separate single grains that have aggregated (e.g. Rea and Hovan, 1995). For an accurate depiction of the size distribution representative of the actual dust signal at the time of deposition (Pye, 1995; Bettis et al., 2003) it is important that these aggregation issues are well understood (Mason et al., 2011; Haberlah and McTainsh, 2011). Wet methods tend to cause the loss of soluble material (e.g. salts), and dissaggregate particles, which is likely to be more applicable far from the source regions, when large particles have fallen out already. Dry methods are appropriate for analyzing recent deposition close to the source areas where the aggregated size of particles is important for understanding deposition processes. In the case of ice sediments most of these problems are negligible, but sample melting is still required for liquid phase analysis with coulter counter or laser devices. Procedures based on ice sublimation and imaging characterization could overcome this step (Iizuka et al., in press), at the price of the uncertainty of imaging techniques for the size distributions (Reid et al., 2003a,b).

In situ sampling strategies include passive sampling devices for dust deposition, such as sediment traps (Clemens, 1998) and ground collectors (Goossens and Rajot, 2008), as well as active or passive atmospheric sampling from ground stations (e.g. Maring et al., 2003), ships (e.g. Stuut et al., 2005) and airplanes (e.g. Ryder et al., 2013a,b).

Dust size information from remote sensing techniques can come from the AERONET stations network, in particular from the stations located in places where the aerosol load is predominantly dust (Huneeus et al., 2011), and have been used for model-data inter-comparisons (e.g. Ginoux et al., 2001; Yu et al., 2009; Albani et al., submitted). Intercomparisons of AERONET remotely sensed data compared with *in situ* measurements in field campaigns provide constraints on the accuracy of the remotely sensed data (e.g. Reid et al., 2003b; Dubovik et al., 2000) A known artifact of AERONET retrievals affects the fine or sub-micron mode of such

Table 1
Overview of techniques for measuring particle sizes and distributions.

Techniques	Principle	Size range	Size resolution	Diameter type	Example references
Sieve-pipette	Geometric + gravimetric	Full range	Coarse: 2–4-8–16-etc. μm	Mass-based	Muhs et al. (2003)
SediGraph	Gravimetric + X-ray attenuation	1–30 μm	Intermediate i.e. 50 channels	Mass-base	Coakley and Syvitski (1991) and Holz et al. (2007)
Coulter Counter/ Elzone	Geometric: volume + electric	0.6–120 μm (sub-range, depending on setup)	Very fine e.g. 256 bins in 0.6–20 μm, but absolute res vary with interval	Volume-based	McTainsh et al., 1997; Delmonte et al., 2002; Clemens, 1998
Laser diffraction	Optical	0.4–120 μm	Intermediate	Volume-based	Buurman et al. (1997), Ruth et al. (2003) and Baumgardner et al. (2001)
Mobility	Electrical mobility	Sub-micron: 3–800 nm	Fine	Number distributions	Weidenohler et al. (2012)
Aerodynamic	Aerodynamic mobility	0.8–30 μm	Intermediate/coarse	Aerodynamic	Reid et al. (2003a,b)
Cascade impactors	Aerodynamic mobility	0.8–30 μm	Intermediate/coarse	Aerodynamic	Reid et al. (2003a,b)
Remote sensing	Optical inversion	0.1–20 μm	Intermediate/coarse	Volume-based	Dubovik and King (2000)

Table 2
Types of size distribution datasets and characterisitics.

	Sediments	In situ sampling	Remote sensing
Time span	$1–10^6$ years	Days-decades	Days-decades
Temporal integration	Subannual-multidecadal	Hours–weeks	Hours
Spatial coverage	Local*	Local**	Local–global
Parameter	Deposition	Deposition, surface concentration	Vertical path/column-integrated
Measurement types	Volumetric, gravimetric, optical, imaging	Volumetric, gravimetric, optical, imaging, aerodynamic	Active/passive Optical path properties

* Spatial representativeness may be large, especially for remote sites (e.g. Mahowald et al., 2011a,b).
** Include aircraft flights and cruises.

inversion products (Dubovik et al., 2000), especially before the particle asimmetricity was taken into account (Dubovik et al., 2006). Detection and evolution of the dust size distribution from satellite is an active area of research and a potentially valuable source of information (Kalashnikova and Kahn, 2008).

Based on the measuring principle, sizing techniques have different sensitivity and resolution across regions of the size spectrum (e.g. Goossens, 2008), so that difficulties emerge when comparing observations (e.g. Reid et al., 2003b; Ryder et al., 2013a,b; Formenti et al., 2011). For example, many sediments studies focused on a wide size range e.g. >100 μm, for which purposes the clay fraction could be treated almost as a unique size class, although studies comparing different techniques showed discrepancies in assessing its relative contribution to the full size spectrum (e.g. Buurman et al., 1997; Goossens, 2008). Nonetheless when it comes to long-range transported dust, finer resolution size is important in assessing distribution shapes and their variability (Steffensen, 1997; Ruth et al., 2003), which is relevant for dust as a proxy of climate processes (McTainsh et al., 1997; Delmonte et al., 2004) and because of the dust size impacts on radiation and clouds (Forster et al., 2007; see also Section 4.1). Lacking a common method of measurement for all of these sources of information is a limitation, although the diversity in the type of observations also offers the opportunity for multiple views of the dust cycle.

Measurements yield size data distributed in discrete channels, which differ depending on the instrument and setup. From the point of view of data dispersal in the literature, there are two main options: parameterized distributions or binned data. In some cases, because of the original goals of specific works, just the median of a distribution was reported, unfortunately hampering broader uses of the measurement's potential information. In general, while observations of dust size distributions exist from a variety of situations, it is difficult to organize all the information in a unique consistent framework.

2.3. Modeling dust size distributions

There are two basic methodologies in use for modeling aerosol size distributions: bin and modal methods. In bin or sectional methods, separate bins for each size of aerosols are simulated separately, allowing them to interact with each other and the gas phase, as well as deposit and be transported (e.g. Su and Toon, 2009). For each bin, however, the size distribution within the bin stays constant, which means there is a constant relationship between mass in the bin and the number of particles. Various numbers of bins can be included from just a few to dozens, depending on the application. In modal models, the mass and number are both carried, which allows the size to evolve with time (Balkanski et al., 1996), and often fewer modes are included (e.g. Liu et al., 2011). In general circulation models, where computational time is a constraint, reduced numbers of bins or modes are usually used. As an example here, we will describe and show results from a 4 bin dust scheme (Mahowald et al., 2006) and a 3-mode modal scheme (Liu et al., 2011)., both of which are implemented in the Community Atmosphere Model (Neale et al., 2013), as described in more detail in (Albani et al., submitted). There are 4 dust bins in the CAM4 version of the model (Albani et al., submitted; Mahowald et al., 2006; Zender et al., 2003). The model assigns dust from an analytic trimodal lognormal probability density function, or three source modes, to four discrete sink modes, or transport bins.

$$M_{i,j} = \frac{1}{2}\left[erf\left(\frac{\ln(D_{max,j}/\tilde{D}_{v,j})}{\sqrt{2}\ln\sigma_{g,i}}\right) - erf\left(\frac{\ln(D_{min,j}/\tilde{D}_{v,j})}{\sqrt{2}\ln\sigma_{g,i}}\right)\right]. \quad (1)$$

The mass overlap, $M_{i,j}$, is computed from the formula above and represents the fraction of mass from each source bin to each transport bin. A modified size distribution following brittle fragmentation theory from Kok (2011) prescribes mass percents of 1.1, 8.7, 27.7,

and 62.5% at every grid point which acts as a source for the 4 bins (0.1–1 μm, 1–2.5 μm, 2.5–5 μm and 5–10 μm) (Albani et al., submitted). The sub-bin size distribution is identical for each bin and is fully described by a lognormal distribution with mass median diameter, $\bar{D}_v = 3.5$ μm and geometric standard deviation, $\sigma_g = 2.0$ (Reid et al., 2003b; Zender et al., 2003). While the mass within each bin changes at each model time step due to deposition processes, the sub-bin size distribution is fixed (Zender et al., 2003). At each time step, the mass in each bin in each grid box is subject to transport or deposition separately, with no interaction between bins. This method is characterized as a bulk aerosol method as all aerosol species are distinct and externally mixed.

Dust size distributions in CAM5 are treated as lognormal modes instead of bins (called the MAM3 or modal aerosol model, with 3 modes) (Albani et al., submitted; Liu et al., 2011). Whereas different particle types were carried in distinctive bins in CAM4, the lognormal modes in CAM5 can carry more than one species, and an intra-mode internal mixture is assumed. More specifically, in MAM3, dust is prescribed in two lognormal modes, an accumulation mode and a coarse mode, where each of these modes is not exclusive to dust but also carries other aerosol species, i.e. sea salt, black carbon, organic carbon, and sulfate. Mixing between modes is assumed to be negligible for dust, however mixing within modes and water uptake changes the mass median diameter and number concentration of the mode while the geometric standard deviation is held constant. The mass median diameter and number concentration are allowed to change within each mode with fixed geometric standard deviation, and cutoff boundaries for the fine dust and coarse dust mode are 0.1–2 μm and 2–10 μm, respectively. Similar to CAM4, dust in the updated model uses Kok (2011) to parameterize the distribution of dust mass between the modes, and the mass percents in each mode are 1.1 and 98.9% for the accumulation and coarse modes, respectively.

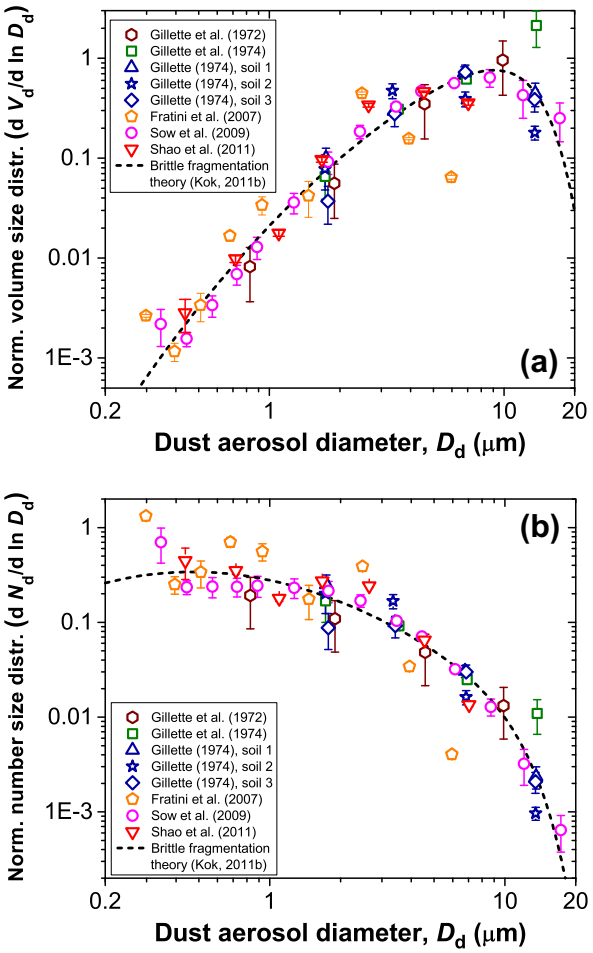

Fig. 3. Compilation of measurements of the volume (A) and number (B) dust size distribution at emission. Measurements by Gillette and colleagues (Gillette, 1974; Gillette et al., 1972, 1974) used optical microscopy, and were taken in Nebraska and Texas. Conversely, measurements by Fratini et al. (2007), Sow et al. (2009), and Shao et al. (2011a) used optical particle counters. These measurements were made in China, Niger, and Australia, respectively. All measurements were normalized following the procedure described in Kok (2011b). Note that the Fratini et al. measurements were normalized over the range of 2–4 μm (instead of 2–10 μm), because the results from the coarser particle bins in that data set are unreliable (Fratini, 2012, personal communication). Furthermore, adjacent pairs of particle bins in the Fratini et al. data were averaged to reduce scatter.

3. Dust size distribution in observations and models

The dust size distribution at emission is extremely important for downwind concentrations, since most of the dust is emitted at sizes that do not effectively grow by condensation or coagulation (Seinfeld and Pandis, 1998) (Section 3.1). Once in the atmosphere, the size distribution evolves due to deposition processes, primarily, as large particles fall out more quickly (Section 3.2). The size evolution of dust can be probed while in the atmosphere, as well as at deposition (Section 3.3).

3.1. The dust size distribution at emission

3.1.1. Observations of the dust size distribution at emission

Accurate representation of the dust particle size distribution (PSD) in the atmosphere begins with a parameterization of the dust PSD at emission. Note that the different measurements of the size distributions at emission are all in rough agreement for dust aerosols smaller than ~5 μm in diameter (Fig. 3). This is quite remarkable, considering that these measurements were taken over different soils, in different source regions, and using different techniques. For larger particles (> ~5 μm), the size distributions do differ substantially, a possible cause of which is discussed in the next section.

In order to parameterize the dust PSD at emission in models, the dependence on wind speed and soil properties, such as soil PSD, needs to be understood. A number of studies have reported measurements of the dust PSD at different values of the wind friction speed $u*$ (Fig. 4). Most of these measurements show no dependence of the dust PSD on the wind speed at emission (Fig. 4; see Kok (2011a) for a statistical analysis). The study of Alfaro et al. (1998a) is an exception to this observation, as this study found a strong dependence of the dust PSD on $u*$ in wind tunnel measurements (Fig. 4I). Such a dependence of the dust PSD on $u*$ is not observed in the wind tunnel experiments of Gillette et al. (1974), nor in most field measurements, and might be due to the used wind tunnel being too short to produce steady state saltation (Alfaro et al., 1998a) similar to that occurring in the field (Kok, 2011a). Another possible exception is the study of Sow et al. (2009), which found more fine particles and fewer coarse particles for an energetic wind event than for two less energetic events. However, dust PSD measurements during each event showed no dependence on wind speed (Sow et al., 2009). Furthermore, the different dust events occurred a year apart such that the measured differences could have been caused by changes in the soil state (Kok, 2011a).

On balance, the measurements (Fig. 4) indicate that the dust PSD is independent of the wind speed at emission. This conclusion is supported by the observation of Reid et al. (2008) that the PSD of dust advected from individual source regions appeared invariant to the wind speed at emission.

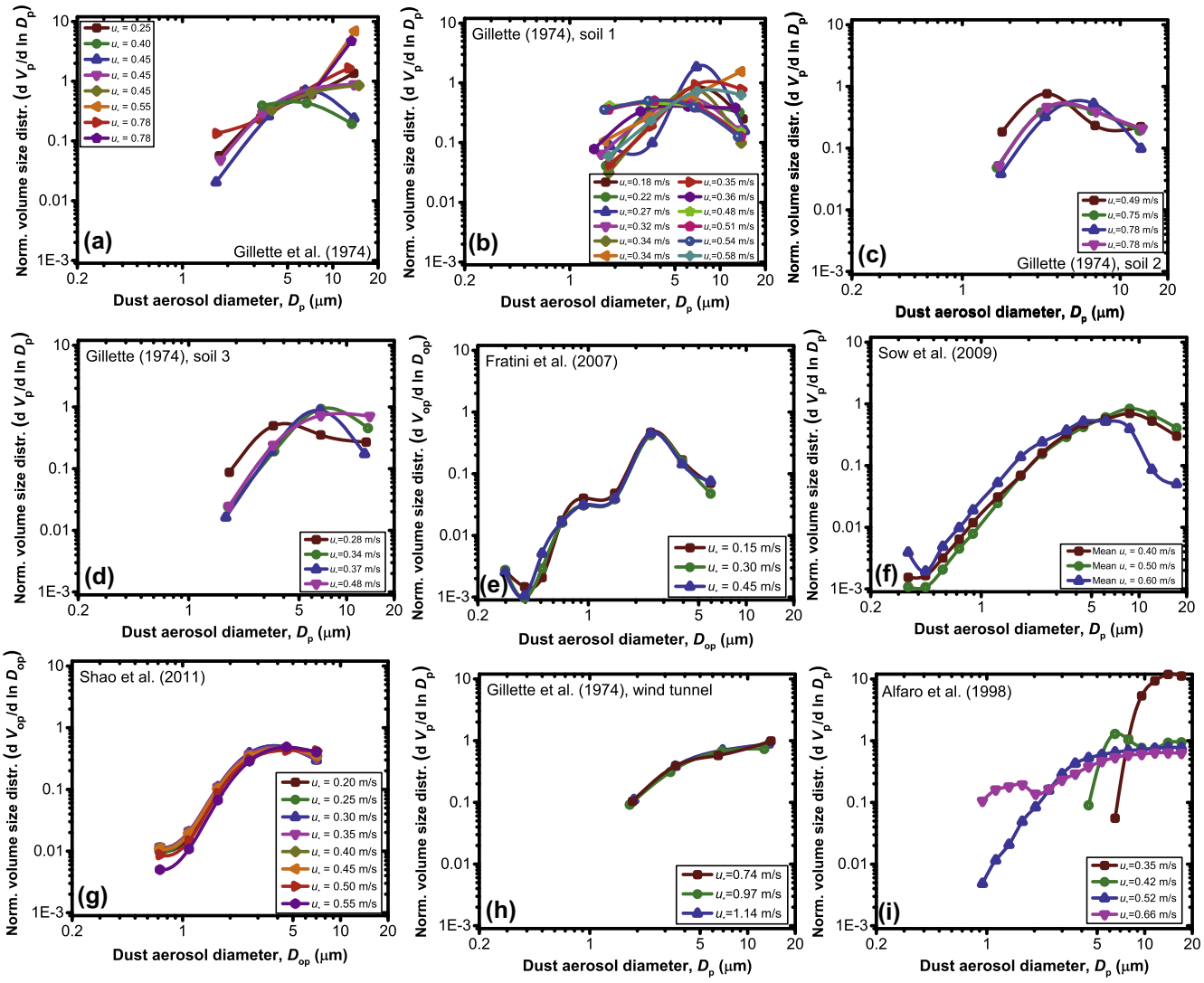

Fig. 4. Compilation of measurements of the dust size distribution at emission measured at different wind friction velocities. Shown are results of the field studies of (A) Gillette et al. (1974), (B–D) soils 1–3 of Gillette (1974), (E) Fratini et al. (2007), (F) Sow et al. (2009), and (G) Shao et al. (2011a). In addition, panels (H) and (I) show results from the wind tunnel measurements of Gillette et al. (1974) and Alfaro et al. (1998a), respectively.

The dependence of the dust PSD at emission on soil properties is more difficult to determine, as few measurements for different soils exist (e.g. DO4Models, http://www.geog.ox.ac.uk/research/climate/projects/do4models.html). However, the available experimental data sets show, as mentioned above, remarkably similar size distributions for $D_p < \sim 5$ μm (see Fig. 3). Since the measurements in Fig. 3 were taken for a range of soil types, this result suggests a limited dependence of the PSD of <5 μm dust on soil properties. This is highly fortuitous for parameterizing the emitted dust size distribution in models, although it should be verified by further measurements.

The different measurements of the PSD of particles >5 μm do show substantial scatter, which is likely largely due to differences in the state and PSD of the soil. Therefore, more research is needed to better quantify the influence of the soil size distribution on the emitted dust size distribution.

3.1.2. Theories and parameterizations of the dust size distribution at emission

As discussed in Section 1, most dust aerosols are emitted into the atmosphere through the mechanical impacts of saltating particles. These impacts create elastic waves that are necessary to rupture the interparticle bonds binding dust particles to other soil particles. The patterns in which these bonds are ruptured determines the size distribution of dust aerosols. The studies of Alfaro and Gomes (2001), Shao (2001, 2004), and Kok (2011b) proposed distinct theories that use this knowledge of the origin of dust aerosols to predict the dust PSD at emission.

The Dust Production Model (DPM), proposed by Alfaro and colleagues (Alfaro et al., 1997; Alfaro and Gomes, 2001), predicts that the mechanical impacts of saltators produce dust particles in three distinct lognormal modes. A critical ingredient of the DPM is that the relative contribution of each of the three modes depends on the bonding energy for each mode. The bonding energy and median diameter of these modes was determined from fitting to wind tunnel experiments (Alfaro et al., 1997), and recent results suggest that these parameters might need to be adjusted for each soil (Sow et al., 2011). Since the DPM assumes that the saltator impact speed scales with wind speed, this model predicts a strong dependence of dust PSD on $u*$. Although an increase of the saltator impact speed with $u*$ is intuitive, recent measurements and theories indicate that the saltator impact speed actually stays constant with $u*$ (Kok et al., 2012). Consequently, the DPM predicts a strong dependence of the emit-

ted dust PSD on $u*$, which is not shown by most measurements (see Fig. 4).

Following the DPM, Shao (2001, 2004) proposed a different theory based on the insight that the emitted dust size distribution is intermediate between the undisturbed and the fully disturbed (i.e., fully disaggregated) soil size distributions. Specifically,

$$P_d(D_p) = \gamma p_m(D_p) + (1-\gamma)p_f(D_p), \quad (2)$$

where p_d, p_m, and p_f denote the size distributions of the emitted dust aerosols, the undisturbed soil, and the fully disturbed soil. The problem then is how to estimate the weighting factor γ; Shao (2001, 2004) postulated that γ increases monotonically with $u*$. However, in more recent work, Shao et al. (2011a) suggested that γ is independent of $u*$, based on the observation that field measurements of the dust PSD show no clear dependence on $u*$ (see Fig. 4G).

Most recently, Kok (2011b) proposed a theory for the size distribution of emitted dust aerosols that assumes that most dust emission is the result of fragmentation of soil dust aggregates by impacting saltators. As also noted by Gill et al. (2006), stressed dry soil aggregates are known to fail as brittle materials (Braunack et al., 1979; Lee and Ingles, 1968; Perfect and Kay, 1995; Zobeck et al., 1999). Therefore, Kok (2011b) hypothesized that the impact energy of a saltating particle shatters aggregates of dust particles in soils in much the same way that glass shatters upon a sufficiently energetic impact. Since the patterns in which cracks are created and eventually merge in brittle materials is *scale-invariant* (Astrom, 2006), and thus does not require detailed knowledge of the strength of interparticle bonds in the dust aggregate, this hypothesis produced a relatively straightforward expression for the size distribution of emitted dust aerosols. Specifically, Kok (2011b) derived

$$\frac{dV_d}{d\ln D_d} = \frac{D_d}{c_v}\left[1 + erf\left(\frac{\ln(D_d/\overline{D_s})}{\sqrt{2}\ln\sigma_s}\right)\right]\exp\left[-\left(\frac{D_d}{\lambda}\right)^3\right], \quad (3)$$

where V_d is the normalized volume of dust aerosols with size D_d, $c_V = 12.62$ μm is a normalization constant, and $\sigma_s \approx 3.0$ and $\bar{D})s \approx 3.4$ μm are the geometric standard deviation and median diameter by volume of the log-normal distribution of a typical arid soil size distribution in the $\leqslant 20$ μm size range. The parameter λ denotes the propagation distance of side branches of cracks created in the dust aggregate by a fragmenting impact, and Kok (2011b) obtained $\lambda = 12 \pm 1$ μm using least-square fitting to dust PSD measurements. Eq. (3) is in surprisingly good agreement with measurements (Fig. 3), and correctly predicts the independence of the emitted dust PSD with $u*$ (Fig. 4). Furthermore, implementation of Eq. (3) into models has improved agreement against measurements in several regional and global models (Albani et al., submitted; Johnson et al., 2012; Nabat et al., 2012; Zhang et al., 2013). This approach assumes that the dust size distribution is not a strong function of soil properties which matches many observations (e.g. Fig. 3), but is not consistent with all observations (e.g. Reid et al., 2003a,b).

Note that the side crack propagation length λ remains highly uncertain. In particular, the recent measurements of Shao et al. (2011a) suggest a smaller value of λ; measurements of Fratini et al. (2007), which were overlooked in Kok (2011b), also suggest a smaller value of λ. However, the coarse particle bins of Fratini et al. (2007) might be unreliable since the cut-off diameter of the inlet system was not determined and might be smaller than the assumed 10 μm (aerodynamic) diameter (Fratini, personal communication, 2012). Considering the large scatter in PSD measurements for dust with diameters > ~5 μm, which is the portion of the theoretical curve that is sensitive to the value of λ, it is likely that the exact value of λ is highly dependent on the properties of the soil (Kok, 2011a).

3.1.3. Treatment in atmospheric circulation models

As discussed in Section 2.2, atmospheric circulation models use either a modal or a sectional (bin) method to represent the dust size distribution at emission and during transport. Following the prevailing treatment of other aerosol species (e.g., sulfates; Seinfeld and Pandis, 1998), many models simulate the dust size distribution as a sum of lognormal modes (e.g., Balkanski et al. (2007), Zhao et al. (2010)). Although this approach is computationally efficient for models using the modal method, measurements of the dust size distribution at emission and *in situ* near source regions do not generally support the idea that the dust PSD at emission is a sum of a few lognormal modes (Figs. 4 and 5).

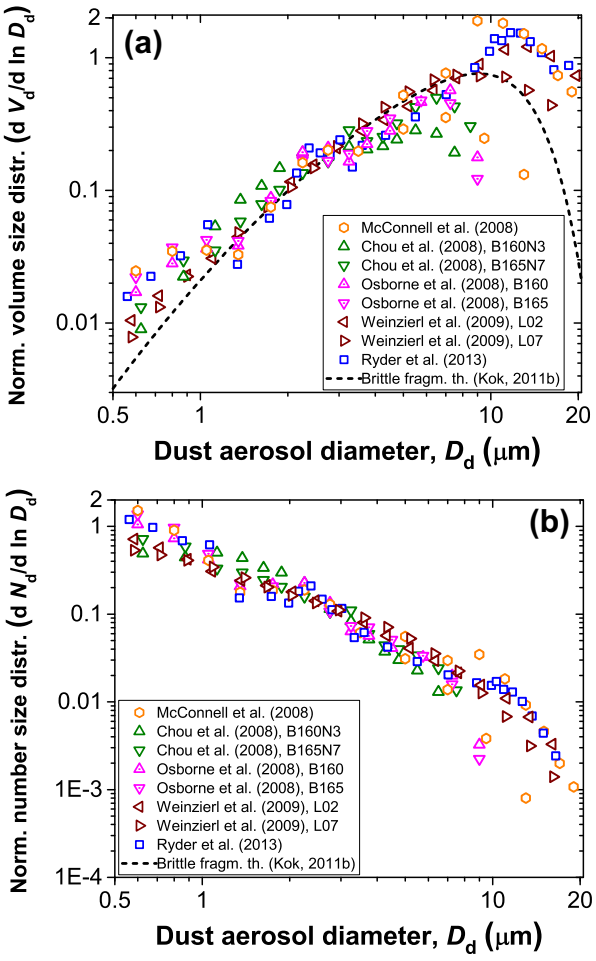

Fig. 5. Compilation of *in situ* measurements of the dust PSD close to North African source regions. Shown are measurements from the DODO (Fig. 7 in McConnell et al. (2008)), DABEX (Fig. 6 in Chou et al. (2008) and Fig. 10 in Osborne et al. (2008)), SAMUM-1 (Fig. 8 in Weinzierl et al. (2009)), and Fennec (Fig. 5 in Ryder et al. (2013b)) field campaigns. Error bars have been omitted to prevent clutter, and can be found in the original references. Only dust PSD measurements of aerosols with diameters >0.5 μm are plotted because a substantial fraction of smaller aerosols are not mineral dust (Chou et al., 2008; Kandler et al., 2009; Weinzierl et al., 2009). Instruments used in determining the dust PSD include electron microscopy (Chou et al., 2008; McConnell et al., 2008) and optical sizing instruments (McConnell et al., 2008; Osborne et al., 2008; Ryder et al., 2013b; Weinzierl et al., 2009). All measured dust PSDs were normalized by fitting the number (N) size distribution to the power law $dN/d\log D_d = cD_d^{-2}$ in the size range 2–4 μm, and dividing all measurements by the fitted proportionality constant c (Kok, 2011b). Measurements from the SHADE (Haywood et al., 2003) and SAMUM-2 (Schladitz et al., 2011) measurement campaigns were not included, since these measurements were not taken over source regions. Measurements from the GERBILS field campaign (Johnson and Osborne, 2011) were also not used, because the measurement ranges of the two used instruments did not overlap, possibly introducing substantial systematic errors.

Many models also include an explicit dependence of the dust size distribution at emission on the soil size distribution (e.g., Ginoux et al., 2001; Tegen and Lacis, 1996), an idea that is supported by theory (see above). However, measurements only show substantial variation in the dust PSD emitted by different soils for dust particles > ~5 μm; the dust PSD for smaller particles shows relatively little variation between soils (Figs. 4 and 5). Many models also include a dependence of the dust PSD on the wind speed at emission (e.g., Ginoux et al., 2001), an idea that is mainly based on the wind tunnel studies of Alfaro et al. (1997, 1998a). However, as discussed above, field measurements show no statistically significant dependence of the dust PSD on u_* (Fig. 4; Kok (2011a)). These results suggests that the dependence of the emitted dust PSD on the soil type and wind speed might be overparameterized in certain models.

3.2. Atmospheric removal processes and dust size

Desert dust particles, like other aerosols, are effectively removed by both wet and dry deposition processes. Both removal processes are size dependent. For removal processes, the lifetime is defined as the amount of mass in the atmosphere divided by the surface flux, and we can define total lifetime to deposition processes, as well as separate lifetimes to wet and dry processes.

Turbulent motions in the atmosphere bring aerosols in the boundary layer down to the surface, as they are transported with the eddies. Close to the surface there is a thin layer of stagnant quasi-laminar air, which the aerosol has to transverse. Once an aerosol makes contact with the ground, it can be deposited onto the surface, called dry deposition. Most often the deposition flux is parameterized as equal to a deposition velocity times the concentration of particles. The deposition velocity is derived using a resistance model, where the deposition velocity is the inverse of the sum of the aerodynamic resistance (from the eddies), quasi-laminar layer resistance, and the canopy resistance of the surface to deposition (Seinfeld and Pandis, 1998).

In addition to this turbulent dry deposition, aerosols can gravitationally settle and deposit on the surface. Because aerosols are solids or liquids suspended in the atmosphere, and thus are less buoyant than the air around them, they accelerate downward. This motion is opposed by friction, and the terminal velocity is the speed at which a particle falls at equilibrium. Larger particles fall much faster than smaller particles, giving them a larger deposition velocity; for example, particles of size 0.1, 1, and 10 μm will have deposition velocities of 0.001, 0.05 and 1 cm/s, respectively, under the same atmospheric conditions (Seinfeld and Pandis, 1998).

The theory of dry deposition that is used in model and data analysis is fairly standard (e.g. Seinfeld and Pandis, 1998), however there have been few detailed field campaigns in the last 30 years that would allow us to verify these theories (e.g. Slinn and Slinn, 1980; Prospero et al., 1996; Schulz et al., 2012), and some measurements along transport pathways indicate a longer lifetime of coarse aerosols than expected from deposition theories (Maring et al., 2003; Ryder et al., 2013a). Because of the different sedimentation rates, there is a strong dependence of dry deposition lifetime onto size (Fig. 6). In addition, the lifetime of dust particles also varies spatially (Fig. 6). This is because the dry deposition removal occurs at the surface, and so occurs more quickly for particles close to the surface, or in bouyant boundary layers (which can extend up to 6 km over desert regions e.g. Mahowald and Dufresne (2004), where the dust can be quickly brought to the surface and deposited.

Wet deposition refers to removal of aerosols during cloud or precipitation processes, which cause the aerosol to be deposited onto the surface. Dust aerosols are readily incorporated into clouds, either as cloud condensation nuclei or ice nuclei, where aerosols are important for the formation of clouds (e.g. DeMott et al., 2003; Rosenfeld and Nirel, 1996), or when the aerosols make contact with the cloud droplets and are captured by the cloud droplets within clouds. While desert dust particles are insoluble, they readily attract water to their surfaces (Koretsky et al., 1997), and can act as cloud condensation nuclei by adsorption of water vapor (Kumar et al., in press). There is also growing evidence that dust aerosols are one of the most important sources of ice nuclei, and thereby can substantially affect cloud processes (Creamean et al., 2013; DeMott et al., 2010). Thus, processing of atmospheric dust particles with sulfate or other pollutants is not necessary for them to be readily incorporated into clouds (e.g. Fan et al., 2004). These cloud droplets can grow to a size (1–100 μm) where their terminal velocity is much larger than for the original aerosols, causing clouds that are in contact with the ground (e.g. fog) to accelerate the deposition of aerosols (e.g. Seinfeld and Pandis, 1998). These processes are called in-cloud scavenging.

Once cloud droplets grow to where their terminal velocities are large enough to cause deposition in minutes (100 μm to 1 mm), they are called rain droplets, and can cause the deposition of aerosols to the surface from high in the atmosphere. Below the cloud, rain drops can hit and collect more aerosols, which is called below-cloud scavenging.

Wet deposition is sometimes parameterized as a simple scavenging rate, where one assumes a constant removal of aerosols per amount of water precipitated (e.g. Tegen and Fung, 1994). However, using surface concentration to infer wet deposition can produce errors in situations where the aerosols are carried in plumes elevated above the boundary layer (e.g. Heimburger et al., 2012). For modeling, there are many more physically based schemes (e.g. Giorgi and Chameides, 1985), but models using different parameterizations produce varying results (e.g. Huneeus et al., 2011; Rasch et al., 2000). There are few measurements of wet deposition processes, implying that there are large uncertainties in model estimates (Huneeus et al., 2011).

Wet deposition is also size dependent. In-cloud scavenging should incorporate most aerosols, especially larger particles, such as most desert dust, that more readily act as CCN or IN (e.g. Cziczo et al., 2013; Dusek et al., 2006) and thus we do not expect strong size-segregation during in-cloud scavenging (Seinfeld and Pandis, 1998). Theory suggests that below-cloud scavenging should be strongly size dependent, with a maximum rates of deposition occurring when particles are close to 1 μm (Seinfeld and Pandis, 1998), although there is limited field data to evaluate theories. Aerosol wet deposition lifetimes are difficult to assess, but are estimated to be close to 1–2 weeks on average (e.g. Balkanski et al., 1993; Huneeus et al., 2011). Wet removal occurs only during precipitation events, but such events cause removal of most of the aerosol load. Overall, the deposition lifetime of aerosols depends on whether there is precipitation at a given time and place, as well as how large and high particles are at that location (e.g. Fig. 7).

Cloud processing of aerosols can also be important for aggregating aerosols, and thereby changing their size distribution, as well as mixing aerosols, causing externally mixed aerosols to become internally mixed (e.g. Seinfeld and Pandis, 1998). If individual aerosols have mixed compositions, these aerosols are referred to as internally mixed aerosols, whereas if each aerosol is unmixed, but is in a mixed population, this is referred to as an externally mixed aerosol population.

3.3. Atmospheric concentration size fraction: observations and models

3.3.1. Measurements of the atmospheric dust size distribution near source areas

In recent years, a range of *in situ* measurements of the dust size distribution have been published, especially of measurements

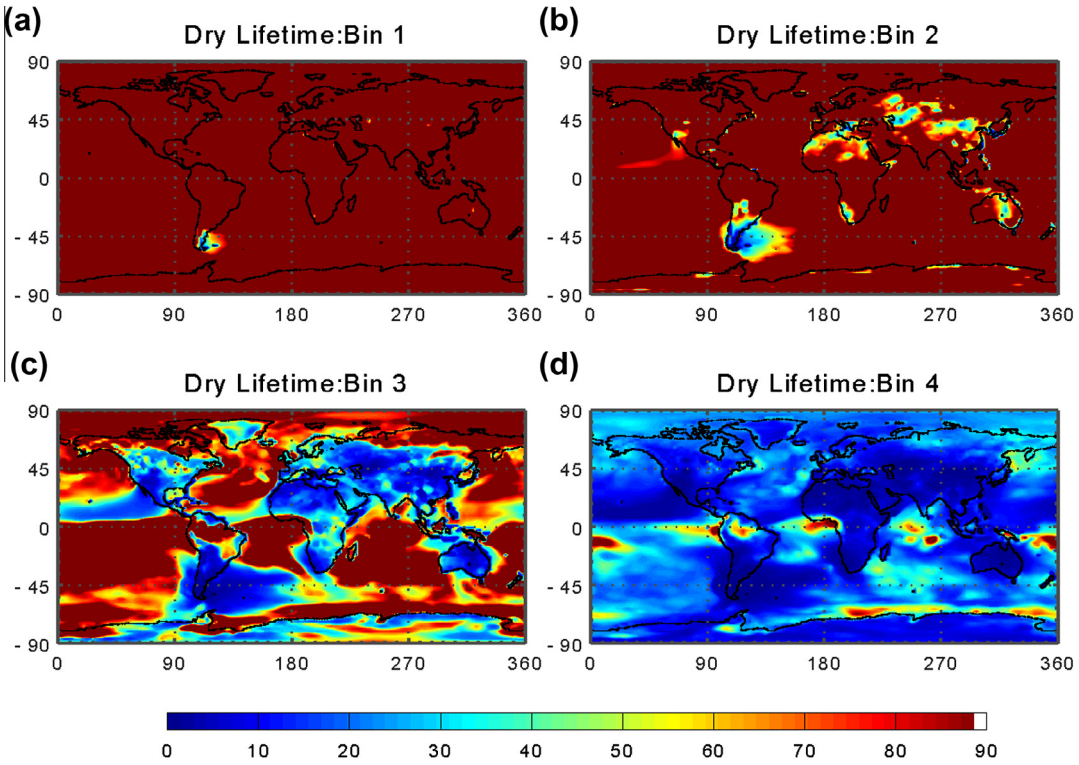

Fig. 6. Spatial distribution of dry deposition lifetimes in CAM4 (Albani et al., submitted) for bins 1–4 (a–d) in days. Dry deposition lifetimes are calculated as the column amount (kg/m^2) divided by the dry deposition flux (kg/m^2/day).

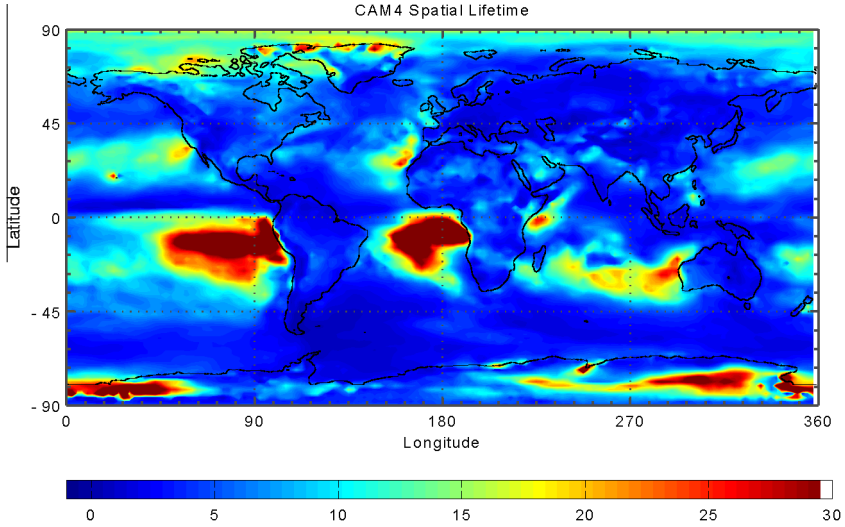

Fig. 7. Desert dust aerosol lifetimes in CAM4 in days (Albani et al., submitted).

close to the North African source regions. These include measurements performed during the SaHAran Dust Experiment (SHADE; Haywood et al. (2003)), Bodele Dust Experiment (BoDEx 2005; Washington et al. (2006), Todd et al. (2007)), the Dust And Biomass Burning Experiment (DABEX; Chou et al. (2008), Osborne et al. (2008)), the Saharan Mineral Dust Experiments (SAMUM-1 and SAMUM-2; Schladitz et al. (2011), Weinzierl et al. (2009)), the Geostationary Earth Radiation Budget Intercomparison of Longwave and Shortwave radiation (GERBILS; Johnson and Osborne (2011)), and the recent Fennec campaign (Ryder et al., 2013b).These field campaigns determined the dust PSD using a variety of optical particle counters, as well as electron microscopy analyses of collected samples. The results of these different campaigns appear consistent for particles between 1 and 5 μm, but differ substantially for the large particle fraction (see Fig. 5). This observation mirrors the results of measurements of the emitted dust size distribution at emission (Fig. 3), and supports the hypothesis that the emission of small dust aerosols (< ~5 μm) is relatively invariant to soil type and state, whereas emission of larger dust aerosols (> ~5 μm) can vary substantially (Kok, 2011a,b). Furthermore, differences in distance from the source will create differences in the gravitational settling rate, which will in turn cause differences mainly in the size distribution of the coarse fraction. Another factor contributing to the scatter in the data for coarser aerosols is that relatively few

PSD measurements are available that extend to coarser sizes, and that the few available measurements of coarser aerosols have larger uncertainty than for finer aerosols because of poor counting statistics (e.g., Ryder et al., 2013b).

Another interesting result from Fig. 3 is that aerosols <1 μm are overrepresented relative to measurements at emission (Fig. 3). This is puzzling since dry deposition is inefficient for particles that small (Miller et al., 2006), and wet deposition is generally insignificant over the Sahara (Ginoux et al., 2001). This apparent discrepancy between *in situ* measurements and measurements at emission could be due to several reasons. First, there could be systematic differences between the size distributions at emission (Fig. 3) and the *in situ* size distributions (Fig. 5), for instance due to systematic differences of soil properties in the Sahara with soils in the measurement locales represented in Fig. 3 (Texas, Niger, China, and Australia). Second, there could be systematic differences in the measurement techniques, although both sets of measurements used a mix of (electron) microscopy and optical sizing instruments. Finally, the *in situ* measurements could contain a substantial fraction of other species of aerosols, especially sulfates (Kandler et al., 2009; Schladitz et al., 2011). The measurements of Chou et al. (2008) and Weinzierl et al. (2009) eliminated volatiles such as sulfates, and these measurements are indeed in closer agreement with measurements at emission than other *in situ* measurements. In particular, the Osborne et al. (2008) measurements, taken during the same flights as the Chou et al. (2008) measurements, show more of an overestimation relative to measurements at emission, supporting this notion.

In addition to measurements near the North African source regions, some field campaigns have determined the dust size distribution near other source regions, such as the Middle East (Reid et al., 2008), as well as dust transported to the Canary Islands, Puerto Rico, and Florida (Maring et al., 2003; Prospero and Custals, 2012; Reid et al., 2003b). The deployment of sun-photometers, including from the AERONET stations, in sites or areas where intensive field campaigns are carried out gives the chance to compare the different measurements. Results from the Puerto Rico Dust Experiment (PRIDE) campaign highlighted how inversion estimates yielded volume median diameter around 4 μm, slightly larger than the more reliable measurements from aerodynamic sizing (3.5 μm), but pointed to large uncertainties (Maring et al., 2003). More recently, size distributions from *in situ* aircraft sampling during the SAMUM-1 and Fennec 2011 campaign showed a significant discrepancy in comparison with AERONET for larger particles (i.e. diameters >6 μm), with the inversions tending towards finer distributions compared to the aircraft samples (Muller et al., 2012; Ryder et al., 2013a,b).

3.3.2. Evolution of dust size distributions: example of North African dust

Close to dust source regions, there is a significant amount of coarse desert dust particles (Figs. 4 and 5), which fall out as the dust travels downwind (Fig. 8). Several observational studies have focused on understanding the evolution of dust size in the North Atlantic (e.g. Reid et al., 1998, 2003b; Maring et al., 2003; Kalashnikova and Kahn, 2008). Here we compare the observed and modeled evolution (from CAM4; Albani et al., submitted). Notice that AERONET data in the smallest size bin are not included, because of possible contamination by other aerosols and large uncertainties (e.g. Albani et al., submitted; Dubovik et al., 2000). In evaluating the model against the different types of observations, one must keep in mind both the different metrics used (geometric vs. aerodynamic diameter, as discussed in 2.1), as well as the differences in measurement techniques (see Figure 20 in Reid et al., 2003a,b). While the model appears to capture the size distribution in the source regions, according to the AERONET observations (Fig. 8c; Albani et al., submitted), and in downwind regions (e.g. Barbados; Fig. 8d), the transition to smaller particles appears to occur too quickly in this model. The loss of the big particles in windblown dust over the Eastern Atlantic is due to preferential settling by dry deposition in the model.

Another important quality of dust size distributions downwind of a large source area is that the atmospheric surface concentrations tend to be finer than the deposition (e.g. Fig. 8f–m), as the bigger particles fall out preferentially. This also helps explain why the surface observations at Izaña (Maring et al., 2003) or for off-shore sampling (Stuut et al., 2005) show a tendency towards a finer distribution than the deposition used as a proxy for dust deposition in marine sediment cores (Mulitza et al., 2010): in fact the deposition observations which are interpreted to be wind-blown show a similar peak as the model just off the coast of Africa (Fig. 8). Also note how the observed size fraction larger than 10 μm is much larger for sea level observations (Stuut et al., 2005) than for a high-elevation site such as Izaña (Maring et al., 2003), although different techniques were used. This analysis supports the use of the coarse mode in the deposition as a proxy for dust variability (e.g. Tjallingii et al., 2008; Mulitza et al., 2010) However, Mulitza et al. (2010) does interpret fine particles in the sediment core as riverine input, although they are in the correct size distribution (0.1–10um) for wind-blown dust from North African sources farther inland.

3.4. Deposition size distribution: observations and models

The size distribution of dust at deposition can be measured through *in situ* observations as well as from paleoarchives (e.g. Fig. 8). Similar to Fig. 7, one can see the dust size distribution evolution during transport towards finer distributions (e.g. Junge, 1977; Derbyshire et al., 1998; Maring et al., 2003; Lawrence and Neff, 2009), and is represented here for a collection of observational estimates of present-day dust deposition (Fig. 8). Larger particles are usually more prevalent close to the source regions, where there are also greater deposition fluxes (Fig. 9). There is a tendency for an inverse relationship between the fraction of coarse particles and dust deposition fluxes in models (Fig. 10) and observations (Fig. 9), although the relationship is not tightly constrained. Notice that the model used here suggests that in the Southern Ocean/Antarctic region, the dust deposition is relatively coarse, which is not seen in the observations (Albani et al., submitted). This is due predominately in the model to South American dust (not shown), and it suggests too many coarse particles are being transported long distances in the model in this region. Because of the lack of observations, it is not clear if this is due to an incorrect source size distribution or if the dry and wet deposition processes in the model are in error.

For paleodust archives, the size distribution is used for many purposes. In some cases the information on size distribution is used to separate aeolian versus riverine inputs (Weltje, 1997; Tjallingii et al., 2008) or highlight sediment redistribution (Rea and Hovan, 1995) in marine sediments, and to contribute to differentiating local versus remote aeolian contributions (Delmonte et al., 2010; Albani et al., 2012a; Marx et al., 2009).

Observed variability in size distribution has been the basis for interpreting changes in the grain size of dust as a paleoclimate proxy, a possible indicator of changes in source area proximity, wind strength and/or changes in the type of deposition processes (e.g. Xiao et al., 1995; Kohfeld and Harrison, 2001; Ruth et al., 2003; Delmonte et al., 2004). For example coarser grain size from loess deposits (Porter and An, 1995) and marine sediments (Hovan et al., 1991) during cold stages have been interpreted in relation to stronger winds – while conversely finer sizes were

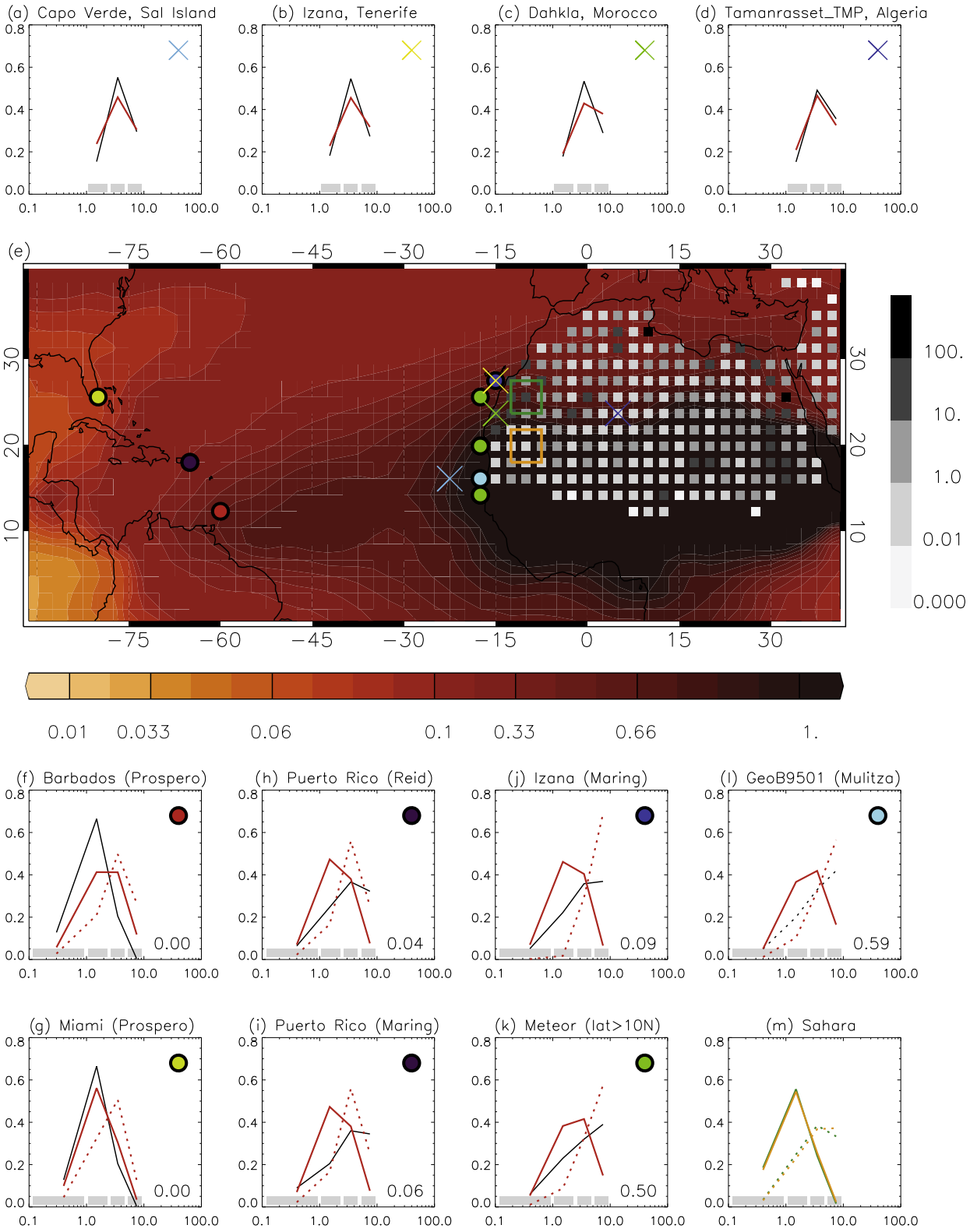

Fig. 8. Evolution of dust size distributions downwind of North Africa. Top panel: column size distributions from AERONET and CAM4 model (Albani et al., submitted) at AERONET sites (a) Capo Verde, (b) Izaña, (c) Dakhla and d) Tamanrasset (marked with x's on map). Modeled and re-binned AERONET size distributions are normalized in the 1–10 μm range according to the model size range as a function of diameter—the grey bars on the x-axis represent the model bins Middle panel: (e) Modeled dust atmospheric surface concentrations in a simulation driven by reanalysis winds for the years 2001–2002 (jja) (red scale, units: $\mu g/m^3$). Squares (grey scale) represent modeled dust emissions (Tg/y) in the reference period. Circles on the map represent observational sites listed in Table 3, the color coding being associated with specific size distribution plots in bottom panel. Bottom panel: comparison of observed (black solid lines) and modeled (red solid lines) size distribution for surface concentrations normalized on the model size range as a function of diameter—the grey bars on the x-axis represent the model bins. Dotted red lines represent modeled dust deposition normalized size distribution. The numbers on the bottom right side of each plot represent the observed fraction larger than 10 μm. (m) (Sahara) represents modeled normalized size distribution of dust surface concentration and deposition in the corresponding regions marked by colored boxes over the source regions.

Table 3
Description and datasets used in construction of Fig. 8.

Site	Sampling period	Techniques	References
Barbados	Apr–Aug 2010–2012	Coulter MultisizerTM 3 using bulk (total) aerosol samples collected on a membrane filters	Prospero and Custals (2012). Particle size distributions of Trade-Wind African dust measured in the air and after dispersal in water. Abstract 1483477 presented at 2012 Fall Meeting, AGU, San Francisco, Calif., 3–7 Dec.
Miami	Apr–Aug 2010–2012	Coulter MultisizerTM 3 using bulk (total) aerosol samples collected on a membrane filters.	Prospero and Custals (2012). Particle size distributions of Trade-Wind African dust measured in the air and after dispersal in water. Abstract 1483477 presented at 2012 Fall Meeting, AGU, San Francisco, Calif., 3–7 Dec.
Puerto Rico	Jul 2000	Aerodynamic diameter	Reid et al. (2003a,b)
Puerto Rico	Jul 2000	Aerodynamic diameter	Maring et al. (2003)
Izana	Jul 1995	Aerodynamic diameter	Maring et al. (2003)
Meteor Cruise M41/1	Feb-Mar 1998	Coulter laser particle sizer (LS230)	Stuut et al. (2005)
GeoB9501	Sample S03.5, age 2002.6 AD	Coulter laser particle sizer (LS230)	Mulitza et al. (2010)

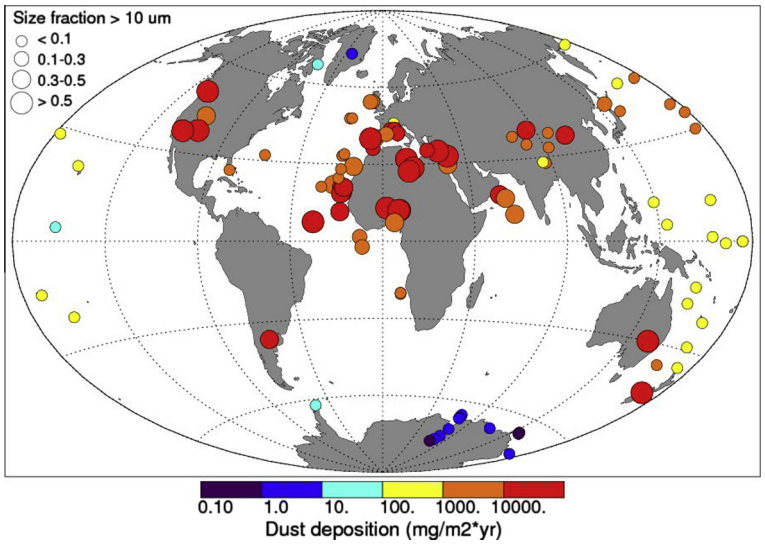

Fig. 9. Deposition flux and size class of present-day dust observational estimates from Albani et al. (submitted). The color scale represent the varying order of magnitude of dust deposition, while the circles radius is proportional to the relative content of coarse (i.e. >10 μm diameter) particles.

associated to increased loess weathering during warmer climate conditions (Guo et al., 1993). Observations from ice cores are centered on a much finer range in the size spectrum, but still showed a similar positive correlation between grain size and cold climates in Greenland (Steffensen, 1997; Ruth et al., 2003), whereas observations in Antarctica indicate opposing behavior in relation to climate conditions depending on the sites (Delmonte et al., 2004).

Since more larger particles would be deposited at a given core if the source moved closer, or if the transported winds were stronger, assuming all other processes remained constant, the paleoclimate interpretation of larger size indicating increased strength of the transporting winds or closer source regions appears appropriate. This assumes that wind strength in source regions does not change size distribution, as indicated by measurements (see Section 2.1.2). However, because of a lack of contemporaneous measurement of winds and size, it has been difficult to use data to test this hypothesis. The AERONET data combined with meteorological station data (see online Supplement for more details), however, give us an opportunity to test this hypothesis relatively close to sources, but not directly in source areas. The results suggest that an increase in wind speed can be associated with a small (0.15 μm) increase in dust particle size downwind of the sources (Fig. 11). This is consistent with the paleoclimate interpretation that stronger winds will carry larger particles.

In addition, changes in precipitation rates and associated changing proportions of dry vs wet deposition in such low-snow accumulation areas such as the Antarctic ice sheet could be a major driver for changing size distributions across different climates (Albani et al., 2012b).

In terms of model-data comparisons, most of the effort so far have focused on the emissions and airborne dust; size distribution of dust deposition has received far less attention, although recent work has started addressing this aspect (e.g. Albani et al., submitted). Climate models also have the potential to assess the alternative causes of the observed dust size variability with climate, and in turn the use of such observations can validate the models' response to changing climates (Albani et al., 2012b).

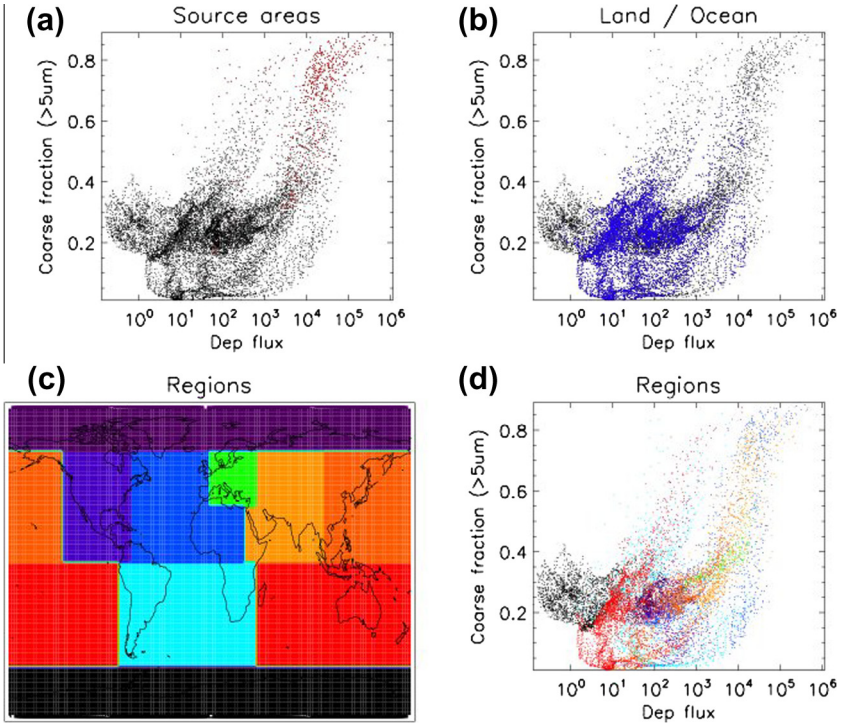

Fig. 10. Scatterplot of fraction of dust >5 μm versus magnitude of dust deposition in CAM4. (a) Source areas (red) versus regions away from sources (black). Source areas are defined here as the model grid cells with dust emissions >0 (b) Ocean areas (blues) versus land regions (black). (c) Regional definitions (c) used in the scatter plot(d), where the colors correspond between (c) and (d).

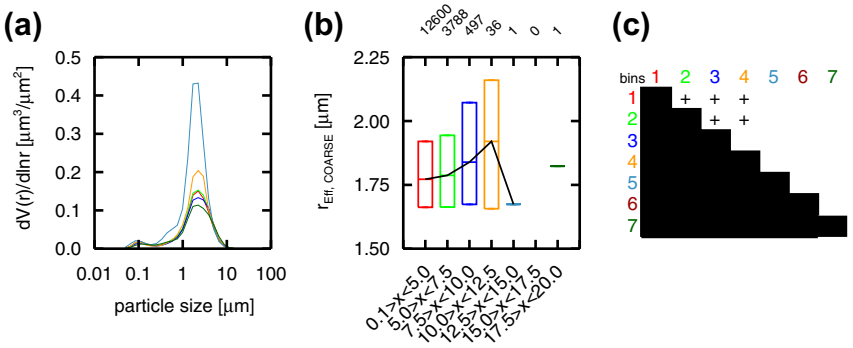

Fig. 11. Relationship between particle size and wind speed derived from 19 AERONET sites and nearby meteorological stations (see online supplement for details). (a) Mean volume particle size distribution for different wind speed classes whereby each color corresponds to the color of the wind speed class presented in plot b. (b) Mean effective radius for the coarse size fraction for different wind speed classes. The number of observations is given above each class on the top axis of the figure. Bars are shown for wind classes with sufficient data for statistical signficance. (c) Plot shows whether the difference in the mean effective radius between the wind speed bins is statistically significant. A plus (minus) symbol indicates a statistically significant increase (decrease) between the mean values. No symbol indicates that the difference is not statistically significant. (For interpretation of the references to colour in this figure legend, the reader is referred to the web version of this article.)

4. Impacts of desert dust and sensitivity to size

4.1. Direct radiative effects dependence on size distribution

Mineral dust is an active component of the climate system, contributing to global radiative balance. Changes in mineral aerosols over the anthropocene are thought to contribute to aerosol radiative forcing (Forster et al., 2007). In this section we focus on the influence that dust size has on the direct effects i.e. the alteration of the atmosphere energy balance by scattering and absorption of electromagnetic radiation in the solar (short-wave: SW) and terrestrial (long-wave: LW) parts of the frequency spectrum. Given the size range of dust particles (>0.1 μm) scattering and absorption in models is described in terms of Mie theory. Assuming homogeneous spherical particles, and based on particle size and wavelength dependent refractive indices of the effective medium, it provides intrinsic optical properties such as the single scattering albedo, mass specific extinction, and asymmetry parameter as a function of the wavelength and particle size (e.g. Tegen and Lacis, 1996). Those optical properties are then used by radiative transfer models to calculate the radiative forcing based on dust mixing ratio distributions in climate models. The accuracy of such representations depends on the representativeness of the discretization of spectral bands and size-dependent optical properties in models with respect to the modeled size distribution of dust aerosols (e.g. Miller et al., 2004). The approximation of particles to spheres is thought to be of second order importance for estimating the radiative flux divergence in climate models, despite its rele-

vance for remote sensing applications (Mishchenko et al., 1995; Dubovik et al., 2002).

Besides the magnitude of dust load, size distribution is a dominant factor in determining the direct radiative forcing (Tegen and Lacis, 1996; Liao and Seinfeld, 1998; Perlwitz et al., 2001). Actually, the relevance of size is tightly related to mineralogical composition in determining the optical properties of dust, as summarized by the size dependence of the refractive indices (e.g. Kandler et al., 2011).

Scattering tends to prevail over absorption in the short wave (SW), as indicated by the observationally derived values >0.9 for the single-scattering albedo (the ratio of scattering efficiency to total extinction efficiency) at visible wavelengths >0.5 μm (Tanré et al., 2001), with smaller particles being the most effective in scattering (e.g. Tegen and Lacis, 1996; Miller et al., 2004). Nonetheless SW absorption is a relevant process throughout the atmospheric column that needs to be considered for an accurate budget of the SW Top-Of-the-Atmosphere (TOA) radiative forcing (e.g. Miller et al., 2004; Balkanski et al., 2007; Yoshioka et al., 2007). On the other hand dust absorption is dominant over scattering in the long wave (LW) especially for super-micron particles, and LW scattering is often not represented explicitly in climate models (e.g. Miller et al., 2006).

The net TOA direct RF from dust eventually depends on the balance between the opposing effects of SW and LW scattering and absorption, where slight variations of the relative magnitude of those factors can significantly alter the overall balance (e.g. Liao and Seinfeld, 1998; Claquin et al., 1998; Albani et al., submitted), as emerging from the large uncertainties in both magnitude and direction (−0.56 to +0.1 W/m^2) of direct dust RF from IPCC AR4 model estimates (Forster et al., 2007). The sensitivity to the SW-LW balance at the TOA needs to be considered also in relation to the evolution of dust size distribution with transport (e.g. Maring et al., 2003), together with changing surface albedo (Carlson and Benjamin, 1980; Li et al., 2004; Patadia et al., 2008 Yoshioka et al., 2007). In fact dust tends to give a positive net surface RF over bright surfaces, being instead negative over dark surfaces such as the oceans (e.g. Miller and Tegen, 1998; Balkanski et al., 2007).

For the estimation of dust direct RF in climate models the primary goal in terms of dust size would be to achieve a good representation in the 1–10 μm range, where most of dust mass with significant lifetimes is concentrated. An additional step would then be to focus on the uncertainties in the small and large tails of the distributions. Small (sub-micron) particles have long lifetimes and are effective scatterers, whereas large particles are LW absorbers with huge mass over source areas (e.g. Ryder et al., 2013a,b). Uncertainties in observational constraints in the magnitude and spatial distribution of dust prevent a full assessment of the importance of dust size to the global RF budget, although the resulting regional effects on e.g. the hydrological cycle (Miller et al., 2004) or atmospheric stability (Luo et al., 2003) can be important.

4.2. Aerosol-cloud indirect effects

As with other aerosol species, dust particles can act as cloud condensation nuclei (CCN) for cloud droplet formation under supersaturated conditions. For a population of dust aerosol in a supersaturated environment, all particles larger than a threshold size, known as the critical diameter, will nucleate cloud droplets (Andreae and Rosenfeld, 2008). This makes the number of dust particles acting as CCN highly sensitive to the ambient (or model predicted) number size distribution(s) shape and median (Karydis et al., 2011).

The critical diameter required for cloud droplet formation depends on the particle solubility, as well as the ambient conditions. Dust particles are often large, increasing their likelihood of exceeding the critical diameter and acting as CCN, and they readily attract water vapor, although insoluble (Koretsky et al., 1997; Karydis et al., 2011).Recent studies suggest that mineral aerosols are the dominant ice nuclei for cirrus clouds (Cziczo et al., 2013). Demott et al. (2010) introduced a scheme for predicting the number of particles that will form ice crystals, known as ice nuclei (IN), based on the ambient temperature and the number concentration of particles with diameters greater than 0.5 μm. They show that much of the variability in IN activity can be explained with this simple relation.

The dual, and competing, roles of dust as CCN and IN cloud our understanding of the global impact of dust on the climate (Mahowald and Kiehl, 2003). Increases in dust acting as CCN would increase cloud albedo and suppress precipitation in warm, stratiform clouds (Rosenfeld et al., 2001), although the global impact of dust in this role is unknown. The impacts of dust on convective clouds are complex and lead to vastly different, even opposite responses in cloud albedo and precipitation (van den Heever et al., 2006). These uncertainties highlight the importance of knowing dust size for predicting CCN and IN and the accompanying climate effects.

4.3. Snow albedo impacts of dust

Dust particles that deposit to snow and ice surfaces reduce their solar albedo, exerting an additional positive RF on the climate system. Albedo reduction from dust occurs primarily in the visible spectrum, where ice absorbs very weakly and snow crystals scatter efficiently. Because scattering is dominated by the ice crystals, factors which determine dust absorptivity, much more so than scattering, determine the RF of dust in snow. These factors include size distribution and imaginary component of the refractive index. While larger particles absorb more solar radiation per particle, the mass-normalized absorption has a non-linear relationship with size, peaking around 0.3 μm in the mid-visible for a typical Saharan dust mixture and wavelength (Fig. 12a). There are Mie resonance features in absorption by individual particles (monodisperse size distributions) that are averaged out in the lognormal size distributions. The albedo reduction caused by a given mass of dust generally peaks close to the radius of maximum 500 nm mass absorption cross-section though deviation from this appears with large dust concentration (Fig. 12b).

Another way in which particle size distribution influences the RF of dust in snow is by determining the mobility of particles with meltwater, and consequently the length of time that the particles alter snow albedo. Several studies have noted that particulate matter becomes concentrated near the snow surface during melt, though few have linked the effectiveness of particle retention to size. Higuchi and Nagoshi (1977) found that dust particles larger than 4–10 μm were relatively immobile with meltwater, while Conway et al. (1996) reported that volcanic ash particles with diameters larger than 5 μm tended to remain near the snow surface during melt. Using Stokes Law to model particle drag, Conway et al. (1996) argue that particles larger than about 6 μm should be immobile with melt fluxes of 500 mm d-1, consistent with observations, while particles smaller than ~1 μm should become mobile when flow rates exceed about 20 mm d^{-1}.

Size distributions of dust in snow depend strongly on proximity to source regions, as discussed previously (Section 3.3). Most of the measurements of dust size distributions in the cryosphere come from ice cores records, used to interpret past climate variability. Measurements from Greenland indicate variations in volume mode radius of ~0.6–1.1 μm throughout the 120ky GRIP core (Steffensen, 1997), ranges in number mean radius of about 0.5–0.7 μm from 10.5–14 kya in the GISP2 core (Zielinski and Mershon, 1997), and variations in volume mode radius of ~0.6–0.85 μm during

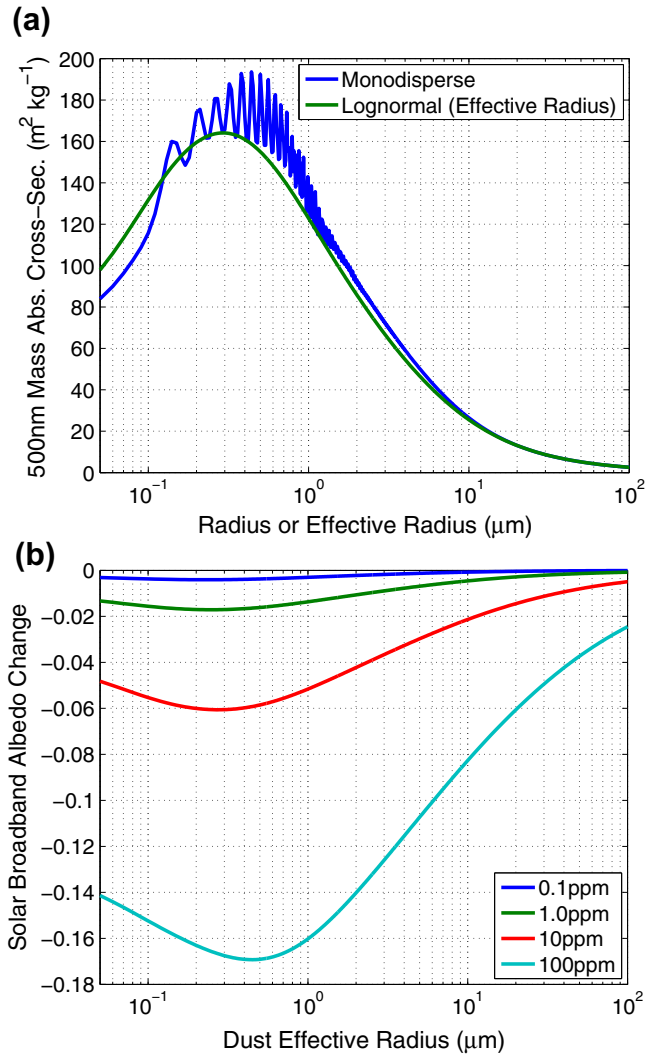

Fig. 12. (a) Mass absorption cross-section (MAC) at 500 nm as a function of particle radius. The green curve depicts MAC as a function of effective radius, or surface area-weighted mean radius. The dust mixture represents the "high hematite" Saharan dust composition described by Balkanski et al. (2007), consisting of 2.7% hematite by volume, 30.3% illite, 24% kaolinite, 23% montmorillonite, 14% quartz, and 6% calcite, and with a density of 2650 kg m^{-3}. The lognormal distribution has geometric standard deviation of 1.8. (b) Simulated hemispheric broadband albedo change of a semi-infinite snowpack as a function of dust effective radius, for different dust mixing ratios in snow. Snow effective grain size is 500 μm and incident sunlight is diffuse. (For interpretation of the references to colour in this figure legend, the reader is referred to the web version of this article.)

9.5–100kya in the NGRIP core (Ruth et al., 2003). Antarctic measurements show ranges in volume mode radius of ~0.9–1.15 μm during the past 21kya from EPICA DOME C in East Antarctica (Delmonte et al., 2002), and a volume mean radius of ~0.85 μm in 20th century ice from James Ross Island (McConnell et al., 2007). Xu et al. (2010) measure larger volume mode radii of 1.6 and 2.1 μm in Mt. Everest ice (dated ~1820 and ~1710), closer to large dust source regions. Very large dust size distributions are measured in mountain snowpack close to local soil sources. In snow samples from the San Juan mountains of Colorado, Neff et al. (2008) found 40% of the dust mass was contained in particle sizes of 10–37 μm, 26% in sizes of 37–63 μm, and 17% in 63–180 μm, while Lawrence et al. (2010) report that 70% of the particles smaller than 250 μm had diameters between 9.3 and 105 μm. Finally, in snow samples collected across China, Wang et al. (2013) found a substantial amount of local soil dust consisting of particles larger than 30 μm.

4.4. Biogeochemistry of dust

Desert dust represents the largest sources of both iron and phosphorus in the atmosphere (Mahowald et al., 2009, 2008). There are large regions of the Southern Ocean and equatorial Pacific that are iron limited (Martin et al., 1991), meaning that the addition of iron allows phytoplankton to grow and increases productivity (e.g. Boyd and Law, 2001). In addition, nitrogen fixing organisms in the ocean may have higher iron requirements (Falkowski et al., 1998), and this would link the nitrogen and iron budgets in the ocean (Moore et al., 2006). Humans are depositing extra nitrogen, phosphorus and iron to the oceans (Duce et al., 2008; Mahowald et al., 2009, 2008), but the most important is the iron deposition for ocean productivity and carbon uptake (Krishnamurthy et al., 2010; Okin et al., 2011). Changes in iron deposition to the ocean have been suggested as an important mechanism for the change in carbon dioxide between the last glacial maximum and the current climate (Kohfeld and Ridgwell, 2009), and may be causing the drawing down of some anthropogenic carbon dioxide today (Mahowald et al., 2010).

Not all iron is bioavailable in the oceans, and although how iron becomes bioavailable is not well understood (Baker and Croot, 2010), there is some evidence that dust size is related to solubility (Baker and Jickells, 2006). Models suggest that the longer lifetime in the atmosphere explains the size dependence of solubility (Hand et al., 2004), although there is also evidence that mineralogy (Journet et al., 2008) or anthropogenic sources may be complicating this picture (Chuang et al., 2005; Guieu et al., 2005). Higher solubilities are also observed at lower total iron concentrations (Sholkovitz et al., 2012).

Productivity in some tropical forests and grassland are phosphorus limited (e.g. Vitousek, 1984; Okin et al., 2008). Since desert dust can be transported across the oceans, and deposited in phosphorus limited regions (Koren et al., 2006; Swap et al., 1992), on geological time scales this phosphorus could maintain productivity (Okin et al., 2004). Over long time scales, the oceans require replenishment of phosphorus (Falkowski et al., 1998), but the likely increased deposition of phosphorus due to humans has not played a large role in ocean biogeochemistry (Krishnamurthy et al., 2010; Okin et al., 2011). The solubility of phosphorus is also likely to be variable (Mahowald et al., 2008), and may be due to differences in solubility at emissions, as well as atmospheric processing by atmospheric acids (e.g. sulfate) (Nenes et al., 2010).

Overall, the evidence suggests that size plays a role in biogeochemistry, largely by modifying how far the particles are transported (e.g. Section 3), but also in the atmospheric processing that occurs on the particles as they travel, and which particles arrive.

5. Summary and Future research needs

The size of desert dust particles is vital to understanding how far they can travel from the source regions, and thus is a critical measurement. Unfortunately desert dust size distributions and their evolution are not well understood. Here we review the state of the science in terms of measurement and modeling methods. There are other important uncertainties in desert dust, including the mass loading, spatial and temporal distribution, as well as their composition, which we did not address in this review (e.g. Zender et al., 2004; Mahowald et al., 2005).

The size of individual particles is to a large extent set at emission, and new measurements and theories roughly agree across a large range (0.1–5 μm), but below and above this range, the size distribution is not well understood. Further measurements are thus needed, in particular to understand the role of changes in soil conditions and soil size distribution. The rates of dry and wet

deposition have established theories, which are commonly used to interpret observations and parameterize models, however, there are few measurements, especially size resolved, of deposition. Since there is also a scarcity of measurements of the evolution of the dust size distribution during transport, we have a generally poor understanding of processes that affect the atmospheric dust size distribution, including deposition and aggregation. The observations of dust aerosols that are available do not consistently show log normal distributions, as often used to model aerosols.

Field campaigns are vital for understanding both size distributions, as well as how to interpret different measurement techniques (e.g. Reid et al., 2003a; Weinzierl et al., 2009; Ryder et al., 2013a,b), and we encourage efforts to embrace size measurements which can be used in sediments for deposition measurements too, which would help produce a consistent view also across time scales and in a wider spatial and environmental domain. Methods based on laser diffraction seem to have the wider applicability ranging from sediment analysis to aircraft measurements, although the technical differences may be relevant. In addition the application of coulter counter measurements to atmospheric samples would help bridging further the gap while having a finer resolution free of assumptions on dust composition (e.g. Ruth et al., 2003) in the fine size range. Better understanding of the role of different sizes on climate and biogeochemistry are important areas of research as well, which have not been fully undrstood.

Currently models do not commonly include dust particles above 10 μm, but a substantial fraction of airborne dust may be above this threshold (Lawrence et al., 2010; Ryder et al., 2013a). This dust is likely important for longwave radiative interactions, as well as for biogeochemistry, even if it does not travel significant distances. Models should improve their ability to capture the evolution of the dust size distribution as the plumes move downwind of the source regions, although this does require more cross-comparison of differing observational methods.

Acknowledgements

We would like to acknowledge funding from NSF (0932946, 1003509, and 1137716) and DOE (DE-SC00006735), and the valuable input of two anonymous reviewers.

Appendix A. Supplementary data

Supplementary data associated with this article can be found, in the online version, at http://dx.doi.org/10.1016/j.aeolia.2013.09.002.

References

Andreae, M.O., Rosenfeld, D., 2008. Aerosol–cloud–precipitation interactions. Part 1. The nature and sources of cloud-active aerosols. Earth-Sci. Rev. 89, 13–41 (doi:10.1016/j.earscirev.2008.03.001).

Albani, S., Delmonte, B., Maggi, V., Baroni, C., Petit, J.R., Stenni, B., Mazzola, C., Frezzotti, M., 2012a. Interpreting last glacial to Holocene dust changes at Talos Dome (East Antarctica): implications for atmospheric variations from regional to hemispheric scales. Clim. Past 8, 741–750 (doi: 10.5194/cp-8-741-2012).

Albani, S., Mahowald, N.M., Delmonte, B., Maggi, V., Winckler, G., 2012b. Comparing modeled and observed changes in mineral dust transport and deposition to Antarctica between the Last Glacial maximum and current climates. Clim. Dyn. 38 (9), 1731–1755 (doi: 10.1007/s00382-011-1139-5).

Albani, S., Mahowald, N.M., Perry, A.T., Scanza, R.A., Zender, C.S., Heavens, N.G., Maggi, V., Kok, J.F., Otto-Bliesner, B.L., submitted. Improved dust representation in the Community Atmospheric Model. J. Adv. Model. Earth Syst.

Alfaro, S.C., Gaudichet, A., Gomes, L., Maille, M., 1997. Modeling the size distribution of a soil aerosol produced by sandblasting. J. Geophys. Res. 102, 11239–11249.

Alfaro, S.C., Gaudichet, A., Gomes, L., Maille, M., 1998a. Mineral aerosol production by wind erosion: aerosol particle sizes and binding energies. Geophys. Res. Lett. 25, 991–994.

Alfaro, S.C., Gaudichet, A., Gomes, L., Maille, M., 1998b. Mineral aerosol production by wind erosion:aerosol particle sizes and binding energies. Geophys. Res. Lett. 25, 991–994.

Alfaro, S.C., Gomes, L., 2001. Modeling mineral aerosol production by wind erosion: emission intensities and aerosol size distributions in source areas. J. Geophys. Res. 106, 18075–18084.

Bagnold, R.A., 1941. The Physics of Blown Sand and Desert Dunes. Methuen, New York.

Baker, A., Croot, P., 2010. Atmospheric and marine controls on aerosol iron solubility in seawater. Mar. Chem. 120, 4–13.

Baker, A., Jickells, T., 2006. Mineral particle size as a control on aerosol iron solubility. Geophys. Res. Lett. 33 (doi: 10.1029/2006GL026557).

Balkanski, Y., Schulz, M., Claquin, T., Guibert, S., 2007. Reevaluation of mineral aerosol radiative forcings suggests a better agreement with satellite and AERONET data. Atmos. Chem. Phys. 7, 81–95.

Balkanski, Y., Schulz, M., Marticorena, B., Bergametti, G., Guelle, W., Dulac, F., Moulin, C., Lambert, C.E., 1996. Importance of the source term and of the size distribution to model the mineral dust cycle. In: Guerzoni, S., Chester, R. (Eds.), The Impact of Desert Dust Across the Mediterranean. Kluwer Academic Publishers, Netherlands, pp. 69–76.

Balkanski, Y.J., Jacob, D.J., Gardner, G.M., Graustein, W.C., Turekian, K.K., 1993. Transport and residence times of tropospheric aerosols inferred from a global three-dimensional simulation of 210Pb. J. Geophys. Res. 98, 20,573–520,586.

Baumgardner, D., Jonsson, H., Dawson, W., O'Connor, D., Newton, R., 2001. The cloud, aerosol and precipitation spectrometer: a new instrument for cloud investigations. Atmos. Res. 59–60, 251–264.

Bettis III, E.A., Muhs, D.R., Roberts, H.M., Wintle, A.G., 2003. Last Glacial loess in the conterminous USA. Quatern. Sci. Rev. 22, 1907–1946.

Boyd, P.W., Law, C.S., 2001. The Southern Ocean Iron RElease Experiment (SOIREE) introduction and summary. Deep-Sea Res. II 48, 2425–2438.

Braunack, M.V., Hewitt, J.S., Dexter, A.R., 1979. Brittle-fracture of soil aggregates and the compaction of aggregate beds. J. Soil Sci. 30, 653.

Brunekreef, B., Holgate, S.T., 2002. Air pollution and health. Lancet 360, 1233–1242.

Buurman, P., Pape, T., Muggler, C.C., 1997. Laser grain-size determination in soil genetic studies 1. Practical problems. Soil Sci. 162 (3), 211–218.

Carlson, Toby.N., Benjamin, Stanley.G., 1980. Radiative Heating Rates for Saharan Dust. J. Atmos. Sci. 37, 193–213. http://dx.doi.org/10.1175/1520-0469(1980)037<0193:RHRFSD>2.0.CO;2.

Chou, C., Formenti, P., Maille, M., Ausset, P., Helas, G., Harrison, M., Osborne, S., 2008. Size distribution, shape, and composition of mineral dust aerosols collected during the African Monsoon Multidisciplinary Analysis Special Observation Period 0: Dust and Biomass-Burning Experiment field campaign in Niger, January 2006. J. Geophys. Res. 113, D00c10.

Chuang, P., Duvall, R., Shafer, M., Schauer, J., 2005. The origin of water soluble particulate iron in the Asian atmospheric outflow. Geophys. Res. Lett. 32 (doi: 10.1029/2004GL021946).

Claquin, T., Schulz, M., Balkanski, Y., Boucher, O., 1998. Uncertainties in assessing radiative forcing by mineral dust. Tellus 50B, 491–505.

Clemens, S.C., 1998. Dust response to seasonal atmospheric forcing: proxy evaluation and calibration. Paleoceanography 13, 471–490.

Coakley, J.P., Syvitski, J.P.M., 1991. Sedigraph techniques. In: Syvitski, J.P.M. (Ed.), Principles, Methods, and Application of Particle Size Analysis. Cambridge University Press, New York, pp. 129–142.

Conway, H., Gades, A., Raymond, C.F., 1996. Albedo of dirty snow during conditions of melt. Water Resour. Res. 32 (6), 1713–1718.

Creamean, J.M., Suski, K.J., Rosenfeld, D., Cazorla, A., DeMott, P.J., Sullivan, R.C., White, A.B., Ralph, F.M., Minnis, P., Comstock, J.M., Tomlinson, J.M., Prather, K.A., 2013. Dust and biological aerosols from the Sahara and Asia influence precipitation in the western US. Science 339, 1572–1578.

Cziczo, D., Froyd, K., Hoose, C., Jensen, E., Diao, M., Zondio, M., Smith, J., Twohy, C.H., Murphy, D.M., 2013. Clarifying the dominant sources and mechansism of cirrus cloud formation. Sci. Express (doi: 10.10126/science.1234145).

Delmonte, B., Petit, J.-R., Andersen, K.K., Basile-Doelsch, I., Maggi, V., Lipenkov, V.Y., 2004. Dust size evidence for opposite regional atmospheric circulation changes over east Antarctica during the last climatic transition. Clim. Dyn. 23, 427–438 (doi: 10.1007/s00382-004-0450-9).

Delmonte, B., Baroni, C., Andersson, P.S., Schöberg, H., Hansson, M., Aciego, S., Petit, J.-R., Albani, S., Mazzola, C., Maggi, V., Frezzotti, M., 2010. Aeolian dust in the Talos Dome ice core (East Antarctica, Pacific/Ross Sea sector): Victoria Land versus remote sources over the last two climate cycles. J. Quat. Sci. 25 (8), 1327–1337.

Delmonte, B., Petit, J.R., Maggi, V., 2002. Glacial to Holocene implications of the new 27,000-year dust record from the EPICA Dome C (East Antarctica) ice core. Clim. Dyn. 18, 647–660 (doi: 10.1007/s00382-001-0193-9).

DeMott, P., Sassen, K., Poellot, M., Baumgardner, D., Rogers, D., Brooks, S., Prenni, A., Kreidenweis, S., 2003. African dust aerosols as atmospheric ice nuclei. Geophys. Res. Lett. 30, 1732 (doi: 1710.1029/2003GL017410).

DeMott, P.J., Prenni, A.J., Liu, X., Kreidenweis, S.M., Petters, M.D., Twohy, C.H., Richardson, M.S., Eidhammer, T., Rogers, D.C., 2010. Predicting global atmospheric ice nuclei distributions and their impacts on climate. Proc. Nat. Acad. Sci. USA 107, 11217–11222.

Derbyshire, E., Meng, X., Kemp, R.A., 1998. Provenance, transport and characteristics of modern Aeolian dust in western Gansu Province, China, and interpretation of the Quaternary loess record. J. Arid Env. 39, 497–516.

Dubovik, O., Holben, B., Eck, T.F., Smirnov, A., Kaufman, Y.J., King, M.D., Tanré, D., Slutsker, I., 2002. Variability of absorption and optical properties of key aerosol types observed in worldwide locations. J. Atmos. Sci., 590–608.
Dubovik, O., King, M.D., 2000. A flexible inversion algorithm for retrieval of aerosol optical properties from Sun and sky radiance measurements. J. Geophys. Res. 105, 20673–20696.
Dubovik, O., Smirnov, A., Holben, B.N., King, M.D., Kaufman, Y.J., Eck, T.F., Slutsker, I., 2000. Accuracy assessments of aerosol optical properties retrieved from Aerososl Robotic Network (AERONET) Sun and sky radiance measurments. J. Geophys. Res. 105, 9791–9806.
Dubovik, O., Sinyuk, A., Lapyonok, T., Holben, B., Mishenko, M., Yang, P., Eck, T.F., Volten, H., Munoz, O., Veihelmann, B., van der Zande, W., Leon, J.-F., Sorokin, M., Slutser, I., 2006. Application of spheroid models to account for aerosol particle nonsphericity in remote sensng of desert dust. J. Geophys. Res. 111. http://dx.doi.org/10.1029/2005JD006619.
Duce, R.A. et al., 2008. Impacts of atmospheric anthropogenic nitrogen on the open ocean. Science 320 (doi: 10.1126/science.1150369).
Dulac, F., Moulin, C., Lambert, C.E., Guillard, F., Poitou, J., Guelle, W., Quetel, C.R., Schneider, X., Ezat, U., 1996. Quantitative remote sensing of African dust transport to the mediterranean. In: Guerzoni, S., Chester, R. (Eds.), The Impact of Desert Dust Across the Mediterranean. Kluwer Academic Publishers, Netherlands, pp. 25–49.
Dusek, U., Frank, G., Hildebrandt, L., Curtis, J., et al., 2006. Size matters more than chemistry for cloud-nucleating ability of aerosol particles. Science 312, 1375–1378.
Falkowski, P.G., Barber, R.T., Smetacek, V., 1998. Biogeochemical controls and feedbacks on ocean primary production. Science 281, 200–206.
Fan, S.-M., Horowitz, L., Levy, H., Moxim, W., 2004. Impact of air pollution on wet deposition of mineral dust aerosols. Geophys. Res. Lett. 31 (doi: 10.1029/2003GL018501).
Formenti, P., Schütz, L., Balkanski, Y., Desboeufs, K., Ebert, M., Kandler, K., Petzold, A., Scheuvens, D., Weinbruch, S., Zhang, D., 2011. Recent progress in understanding physical and chemical properties of African and Asian mineral dust. Atmos. Chem. Phys. 11, 8231–8256.
P. Forster, Ramaswamy, V., Artaxo, P., Berntsen, T., Betts, R., Fahey, D.W., Haywood, J., Lean, J., Lowe, D.C., Myhre, G., Nganga, J., Prinn, R., Raga, G., Schulz, M., Dorland, R.V., 2007. Changes in atmospheric constituents and in radiative forcing. In: Solomon, S., Qin, D., Manning, M., Chen, Z., Marquis, M., Averyt, K.B., Tignor, M., and Miller, H.L. (Eds.), Climate Change 2007: The Physical Science Basis, Contribution of Working Group I to the Fourth Assessment Report of the Intergovernmental Panel on Climate Change, Cambridge University Press, Cambridge, UK and New York, NY, USA, pp. 130–234.
Fratini, G., Ciccioli, P., Febo, A., Forgione, A., Valentini, R., 2007. Size-segregated fluxes of mineral dust from a desert area of northern China by eddy covariance. Atmos. Chem. Phys. 7, 2839–2854.
Gill, T.E., Zobeck, T.M., Stout, J.E., 2006. Technologies for laboratory generation of dust from geological materials. J. Hazard. Mater. 132, 1–13.
Gillette, D.A., 1974. On the production of soil wind erosion having the potential for long range transport. J. Rech. Atmos. 8, 734–744.
Gillette, D.A., Blifford, I.H., Fenster, C.R., 1972. Measurements of aerosol size distributions and vertical fluxes of aerosols on land subject to wind erosion. J. Appl. Meteorol. 11, 977–987.
Gillette, D.A., Blifford, I.H., Fryrear, D.W., 1974. Influence of wind velocity on size distributions of aerosols generated by wind erosion of soils. J. Geophys. Res. 79, 4068–4075.
Ginoux, P., Chin, M., Tegen, I., Prospero, J.M., Holben, B., Dubovik, O., Lin, S.J., 2001. Sources and distributions of dust aerosols simulated with the GOCART model. J. Geophys. Res. 106, 20255–20273.
Ginoux, P., Prospero, J., Gill, T.E., Hsu, N.C., Zhao, M., 2012. Global scale attribution of anthropogenic and natural dust sources and their emission rates based on MODIS deep blue aerosol products. Rev. Geophys. 50 (doi: 10.1029/2012RG000388).
Giorgi, F., Chameides, W.L., 1985. The rainout parameterization in a photochemical model. J. Geophys. Res. 90, 7872–7880.
Goossens, D., 2008. Techniques to measure grain-size distributions of loamy sediments: a comparative study of ten instruments for wet analysis. Sedimentology 55, 65–96.
Goossens, D., Rajot, J.L., 2008. Techniques to measure the dry Aeolian deposition of dust in arid and semi-arid landscapes: a comparative study in West Niger. Earth Surf. Processes Landforms 33, 178–195.
Grousset, F.E., Ginoux, P., Bory, A., Biscaye, P.E., 2003. Case study of a chinese dust plume reaching the French Alps. Geophys. Res. Lett. 30, 1277 (doi: 1210.1029/2002/gl016833).
Guieu, C., Bonnet, S., Wagener, T., Loye-Pilot, M.-D., 2005. Biomass burning as a source of dissolved iron to the open ocean? Geophys. Res. Lett. 22, L19608, doi:19610.11029/12005GL022962.
Guo, Z., Fedoroff, N., An, Z.S., Liu, T.S., 1993. Interglacial dustfall and origin of iron oxides-hydroxides in the paleosols of the Xifeng loess section, China. Sci. Geol. Sin. 2, 91–100.
Haberlah, D., McTainsh, G.H., 2011. Quantifying particle aggregation in sediments. Sedimentology 58, 1208–1216.
Hand, J., Mahowald, N., Chen, Y., Siefert, R., Luo, C., Subramaniam, A., Fung, I., 2004. Estimates of soluble iron from observations and a global mineral aerosol model: biogeochemical implications. J. Geophys. Res. 109, D17205, 17210.11029/12004JD004574.
Haywood, J., Francis, P., Osborne, S., Glew, M., Loeb, N., Highwood, E., Tanre, D., Myhre, G., Formenti, P., Hirst, E., 2003. Radiative properties and direct radiative effect of Saharan dust measured by the C-130 aircraft during SHADE: 1. Solar spectrum. J. Geophys. Res. 108.
Heimburger, A., Losno, R., Triquet, S., Dulac, F., Mahowald, N., 2012. Direct measurement of atmospheric iron, cobalt and aluminum-derived dust deposition at Kerguelen Islands. Global Biogeochem. Cycles 26 (doi: 10.1029/2012GB004301).
Higuchi, K., Nagoshi, A., 1977. Effect of particulate matter in surface snow layers on the albedo of perennial snow patches, in Isotopes and Impurities in Snow and Ice, IAHS-AISH Publ No. 118, pp. 95–97.
Hinds, W.C., 1999. Aerosol Technology: Properties, Behavior, and measurement of Airborne Particles, second ed. John Wiley & Sons, New York.
Holz, C., Stuut, J.-B.W., Henrich, R., Meggers, H., 2007. Variability in terrigenous sedimentation processes off northwest Africa and its relation to climate changes: inferences from grain-size distributions of a Holocene marine sediment record. Sed. Geol. 202 (3), 499–508.
Hovan, S.A., Rea, D.K., Pisias, N.G., 1991. Late Pleistocene continental climate and oceanic variability recorded in Northwest Pacific sediments. Paleoceanography 6 (3), 349–370 (doi: 10.1029/91PA00559).
Huneeus, N., Schulz, M., Balkanski, Y., Griesfeller, J., Kinne, S., Prospero, J., Bauer, S., Boucher, O., Chin, M., Dentener, F., Diehl, T., Easter, R., Fillmore, D., Ghan, S., Ginoux, P., Grini, A., Horowitz, L., Koch, D., Krol, M.C., Landing, W., Liu, X., Mahowald, N., Miller, R., Morccrette, J.-J., Myhre, G., Penner, J., Perlwitz, J., Siter, P., Takemura, T., Zender, C., 2011. Global dust model intercomparison in AEROCOM. Atmos. Chem. Phys. 11, 1–36.
Iizuka, Y., Delmonte, B., Oyabu, I., Karlin, T., Maggi, V., Albani, S., Fukui, M., Hondoh, T., Hansson, M., in press. Sulfate and chloride aerosols during Holocene and last glacial periods preserved in the Talos Dome Ice Core, a peripheral region of Antarctica. Tellus B.
Jickells, T., An, Z., Andersen, K., Baker, A., Bergametti, G., Brooks, N., Cao, J., Boyd, P., Duce, R., Hunter, K., Kawahata, H., Kubilay, N., laRoche, J., Liss, P., Mahowald, N., Prospero, J., Ridgwell, A., Tegen, I., Torres, R., 2005. Global iron connections between dust, ocean biogeochemistry and climate. Science 308, 67–71.
Johnson, B.T., Osborne, S.R., 2011. Physical and optical properties of mineral dust aerosol measured by aircraft during the GERBILS campaign. Q. J. Roy. Meteorol. Soc. 137, 1117–1130.
Johnson, M.S., Meskhidze, N., Kiliyanpilakkil, V.P., 2012. A global comparison of GEOS-Chem-predicted and remotely-sensed mineral dust aerosol optical depth and extinction profiles. J. Adv. Model. Earth Syst. 4.
Journet, E., Desbouefs, K., Caqineau, S., Colin, J.-L., 2008. Mineralogy as a critical factor of dust iron solubility. Geophys. Res. Lett. 35 (doi: 10.1029/2007GL031589).
Junge, C.E., 1977. Processes responsible for the trace content in precipitation. In: Isotopes and impurities in ice and snow, IAHSAISH Publ. 118, Int. Assoc. Hydrol. Sci. Grenoble.
Kandler, D., Schutz, L., Jackel, S., Lieke, K., Emmel, C., Mueller-Ebert, D., Ebert, M., Scheuvens, D., Schladitz, A., Segvic, B., Wiedensohler, A., Weinbruch, S., 2011. Ground-based off-line aerosol measurements at Praia, Cape Verde during the Saharan Mineral Dust Experiment: microphysical properties and mineralogy. Tellus B 63, 459–474.
Kohfeld, K.E., Harrison, S.P., 2001. DIRTMAP: the geological record of dust. Earth-Sci. Rev. 54, 81–114.
Kalashnikova, O., Kahn, R.A., 2008. Mineral dust plume evolution over the Atlantic from MISR and MODIS aerosol retrievals. J. Geophys. Res. 113 (doi: 10.1029/2008JD010083).
Kandler, K., Schutz, L., Deutscher, C., Ebert, M., Hofmann, H., Jackel, S., Jaenicke, R., Knippertz, P., Lieke, K., Massling, A., Petzold, A., Schladitz, A., Weinzierl, B., Wiedensohler, A., Zorn, S., Weinbruch, S., 2009. Size distribution, mass concentration, chemical and mineralogical composition and derived optical parameters of the boundary layer aerosol at Tinfou, Morocco, during SAMUM 2006. Tellus Ser. B-Chem. Phys. Meteorol. 61, 32–50.
Karydis, V.A., Kumar, P., Barahona, D., Sokolik, I.N., and Nenes, A. 2011. On the effect of dust particles on global cloud condensation nuclei and cloud droplet number. J. Geophys. Res.-Atmos. 116, D23, doi:10.1029/2011JD016283.
Kohfeld, K., Ridgwell, A., 2009. Glacial-interglacial variability in atmospheric CO_2, Surface ocean-lower atmosphere processes. Am Geophys. Union, 251–286.
Kok, J.F., 2011a. Does the size distribution of mineral dust aerosols depend on the wind speed at emission? Atmos. Chem. Phys. 11, 10149–10156.
Kok, J.F., 2011b. A scaling theory for the size distribution of emitted dust aerosols suggests climate models underestimate the size of the global dust cycle. Proc. Nat. Acad. Sci. USA 108, 1016–1021.
Kok, J.F., Parteli, E.J.R., Michaels, T.I., Karam, D.B., 2012. The physics of wind-blown sand and dust. Rep. Prog. Phys. 75, 106901.
Koren, I., Kaufman, Y., Washington, R., Todd, M., Rudich, Y., Martins, J., Rosenfeld, D., 2006. The Bodele depression: a single spot in the Sahara that provides most o fhte mineral dust to the Amazon forest. Environ. Res. Lett. 1 (doi: 10.1088/1748-9326/1081/014005).
Koretsky, C., Sverjensky, D., Salisbury, J., D'Aria, D., 1997. Detection of surface hydroxyl speies on quart, gamma-alumina and feldspars using diffuse reflectance infrared spectroscopy. Geochim. Cosmochim. Acta 61, 2193–2210.
Krishnamurthy, A., Moore, J.K., Mahowald, N., Luo, C., Zender, C.S., 2010. The Impacts of atmospheric nutrient inputs on marine biogeochemistry. J. Geophys. Res. 115 (doi: 10.1029/2009JG001115).
Kumar, P., Nenes, A., Sokolik, I., in press. The importance of adsoption for CCN activity and hygroscopic properties of mineral dust aerosol. Geophy. Res. Lett.
Lawrence, C.R., Neff, J.C., 2009. The contemporary physical and chemical flux of Aeolian dust: a synthesis of direct measurements of dust deposition. Chem. Geol. 257, 46–63.

Lawrence, C.R., Painter, T.H., Landry, C.C., Neff, J.C., 2010. Contemporary geochemical composition and flux of aeolian dust to the San Juan Mountains, Colorado, United States. J. Geophys. Res.-Biogeosci. 115.
Lee, I.K., Ingles, O.G., 1968. Soil mechanics selected topics. In: Lee, I.K. (Ed.), The Brittle Failure of Unsaturated Soils, Stabilized Soils, and Rocks. Elsevier, New York, pp. 251–294.
Li, F., Vogelman, A., Ramanathan, V., 2004. Saharan dust aerosol radiative forcing measured from space. J. Clim. 17, 2558–2571.
Liao, H., Seinfeld, J.H., 1998. Radiative forcing by mineral dust aerosols: sensitivity to key variables. J. Geophys. Res. 103, 31637–31645.
Lim, J., Matsumoto, E., 2008. Estimation of aeolian dust flux on Cheju Island, Korea, during the Mid- to Late Holocene. Quatern. Int. 176–177, 104–111.
Liu, X., Easter, R., Ghan, S., Zaveri, R., Rasch, P., Shi, X., Lamarque, J.-F., Gettelman, A., Morrison, H., Vitt, F., Conley, A., Park, S., Neale, R., Hannay, C., Eckman, A., Hess, P., Mahowald, N., Collins, W., Iacono, M., Bretherton, C., Flanner, M., Mitchell, D., 2011. Toward a minimal representation of aerosol direct and indirect effects: model description and evaluation. Geosci. Model Dev. Discuss. 4, 3485–3598.
Luo, C., Mahowald, N., Corral, J.d., 2003. Sensitivity study of meteorological parameters on mineral aerosol mobilization, transport and idstribution. J. Geophys. Res. 108 (4447), 44. http://dx.doi.org/10.1029/2003JD0003483.
Maher, B.A., Prospero, J.M., Mackie, D., Gaiero, D., Hesse, P.P., Balkanski, Y., 2010. Global connections between aeolian dust, climate and ocean biogeochemistry at the present day and at the last glacial maximum. Earth Sci. Rev. 99, 61–97.
Mahowald, N., Baker, A., Bergametti, G., Brooks, N., Duce, R., Jickells, T., Kubilay, N., Prospero, J., Tegen, I., 2005. The atmospheric global dust cycle and iron inputs to the ocean. Global Biogeochem. Cycles 19, GB4025, 4010.1029/2004GB002402.
Mahowald, N., Muhs, D., Levis, S., Rasch, P., Yoshioka, M., Zender, C., 2006. Change in atmospheric mineral aerosols in response to climate: last glacial period, pre-industrial, modern and doubled-carbon dioxide climates. J. Geophys. Res. 111, D10202 (doi: 10210.11029/12005JD006653).
Mahowald, N., Albani, S., Engelstaedter, S., Winckler, G., Goman, M., 2011a. Model insight into glacial-interglacial paleodust records. Quat. Sci. Rev. 30 (7–8), 832–854.
Mahowald, N., Ward, Daniel S., Kloster, Silvia, Flanner, Mark G., Heald, Colette L., Heavens, Nicholas G., Hess, Peter G., Lamarque, Jean-Francois, Chuang, Patrick Y., 2011b. Aerosol impacts on climate and biogeochemistry. Annu. Rev. Environ. Resour. 36, 45–74.
Mahowald, N., Engelstaedter, S., Luo, Chao, Sealy, Andrea, Artaxo, Paulo, Benitez-Nelson, Claudia, Bonnet, Sophie, Chen, Ying, Chuang, Patrick Y., Cohen, David D., Dulac, Francois, Herut, Barak, Johansen, Anne M., Kubilay, Nilgun, Losno, Remi, Maenhaut, Willy, Paytan, Adina., Prospero, Joseph M., Shank, Lindsay M., Siefert, R.L., 2009. Atmospheric Iron deposition: global distribution, variability and human perturbations. Annu. Rev. Mar. Sci. 1, 245–278 (doi: 210.1146/annurev/marine.010908.163727).
Mahowald, N., Jickells, T.D., Alex R. Baker, P.A., Claudia R. Benitez-Nelson, Gilles Bergametti, Tami C. Bond, Ying Chen, David D. Cohen, Barak Herut, Nilgun Kubilay, Remi Losno, Chao Luo, Willy Maenhaut, Kenneth A. McGee, Gregory S. Okin, Ronald L. Siefert, Seigen Tsukuda, 2008. The global distribution of atmospheric phosphorus deposition and anthropogenic impacts. Global Biogeochem. Cycles 22, doi:10.1029/2008GB003240.
Mahowald, N., Kiehl, L., 2003. Mineral aerosol and cloud interactiocns. Geophys. Res. Lett. 30, 10.109/2002GL016762.
Mahowald, N., Kloster, S., Engelstaedter, S., Moore, J.K., Mukhopadhyay, S., McConnell, Albani S., Doney, S., Bhattacharya, A., Curran, M., Flanner, M., Hoffman, F., Lawrence, D., Lindsay, K., Mayewski, P., Neff, J., Rothenberg, D., Thomas, E., Thornton, P., Zender, C., 2010. Observed 20th century desert dust variability: impact on climate and biogeochemistry. Atmos. Chem. Phys. 10, 10875–10893.
Mahowald, N., Dufresne, J.-L., 2004. Sensitivity of TOMS aerosol index to boundary layer height: implications for detection of mineral aerosol sources. Geophys. Res. Lett. 31 (doi: 10.1029/2003GL018865).
Maring, J., Savoie, D., Izaguirre, M., Custals, L., Reid, J., 2003. Mineral dust aerosol size distribution change during atmospheric transport. J. Geophys. Res. 108, 8592.
Marticorena, B., Bergametti, G., 1995. Modeling the atmospheric dust cycle: 1. Design of a soil-derived dust emission scheme. J. Geophys. Res. 100, 16,415–416,430.
Martin, J., Gordon, R.M., Fitzwater, S.E., 1991. The case for iron. Limnol. Oceanogr. 36, 1793–1802.
Marx, S.K., McGowan, H.A., Kamber, B.S., 2009. Long-range dust transport from eastern Australia: a proxy for Holocene aridity and ENSO-type climate variability. Earth Planet. Sci. Lett. 282, 167–177.
Mason, J.A., Greene, R.S.B., Joeckel, R.M., 2011. Laser diffraction analysis of the disintegration of Aeolian sedimentary aggregates in water. Catena 87, 107–118.
McConnell, C.L., Highwood, E.J., Coe, H., Formenti, P., Anderson, B., Osborne, S., Nava, S., Desboeufs, K., Chen, G., Harrison, M.A.J., 2008. Seasonal variations of the physical and optical characteristics of Saharan dust: Results from the Dust Outflow and Deposition to the Ocean (DODO) experiment. J. Geophys. Res. 113.
McConnell, J.R., Aristarain, A.J., Banta, J.R., Edwards, P.R., Simões, J.C., 2007. 20th Century doubling in dust archived in an Antarctic Peninsula ice core parallels climate change and desertification in South America. Proc. Nat. Acad. Sci. 104 (14), 5743–5748 (doi: 10.1073/pnas.0607657104).
McTainsh, G.H., Lynch, A.W., Hales, R., 1997. Particle-size analysis of aeolian dusts, soils and sediments in very small quantities using a Coulter Multisizer. Earth Surf. Proc. Land. 22 (13), 1207–1216.
Miller, R., Tegen, I., 1998. Climate response to soil dust aerosols. Am. Meteorl. Soc. 11, 3247–3267.
Miller, R., Tegen, I., Perlwitz, J., 2004. Surface radiative forcing by soil dust aerosols and the hydrologic cycle. J. Geophys. Res. 109. http://dx.doi.org/10.1029/2003JD004085.
Miller, R.L., Cakmur, R.V., Perlwitz, J., Geogdzhayev, I.V., Ginoux, P., Koch, D., Kohfeld, K.E., Prigent, C., Ruedy, R., Schmidt, G.A., Tegen, I., 2006. Mineral dust aerosols in the NASA goddard institute for space sciences ModelE atmospheric general circulation model. J. Geophys. Res. 111, D06208.
Mishenko, M., Lacis, A., Carlson, B., Travis, L., 1995. Nonsphericity of dust-like tropospheric aerosols: implications for aerosol remote sensing and climate modeling. Geophys. Res. Lett. 22. http://dx.doi.org/10.1029/1095GL00798.
Moore, J.K., Doney, S., Lindsay, K., Mahowald, N., Michaels, A., 2006. Nitrogen fixation amplifies the ocean biogeochemical response to decadal timesclae variations in mineral dust deposition. Tellus 58B, 560–572.
Muhs, D.R., Ager, T.A., Bettis III, E.A., McGeehin, J., Been, J.M., Begét, J.A., Pavich, M.J., Stafford Jr., T.W., Stevens, D.A.S.P., 2003. Stratigraphy and palaeoclimatic significance of late quaternary loess–palaeosol sequences of the last interglacial–glacial cycle in central Alaska. Quatern. Sci. Rev. 22, 1947–1986.
Mulitza, S., Heslop, D., Pittauerova, D., Fischer, H., Meyer, I., Stuut, J.-B., Zabel, M., Mollenhauer, G., Collins, J., Kuhnert, H., Schulz, M., 2010. Increase in African dust flux at the onset of commercial agriculture in the Sahel region. Nature 466 (doi: 10.1038/nature09213, 09226-09228).
Muller, D., Lee, K.H., Gasteiger, J., Tesche, M., Weinzierl, B., Kandler, K., Muller, T., Toledano, C., Otto, S., Althausen, D., Ansmann, A., 2012. Comparison of optical and microphysical properties of pure Saharan mineral dust observed with AERONET Sun photometer, Raman lidar, and in situ instruments during SAMUM 2006. J. Geophys. Res. 117, 25.
Nabat, P., Solmon, F., Mallet, M., Kok, J.F., Somot, S., 2012. Dust emission size distribution impact on aerosol budget and radiative forcing over the Mediterranean region: a regional climate model approach. Atmos. Chem. Phys. 12, 10545–10567.
Neale, Richard B., Jadwiga Richter, Sungsu Park, Peter H. Lauritzen, Stephen J. Vavrus, Philip J. Rasch, Minghua Zhang, 2013: The Mean Climate of the Community Atmosphere Model (CAM4) in Forced SST and Fully Coupled Experiments. J. Clim., 26, 5150–5168. http://dx.doi.org/10.1175/JCLI-D-12-00236.1.
Neff, J.C. et al., 2008. Increasing eolian dust deposition in the western United States linked to human activity. Nat. Geosci. 1 (3), 189–195 (doi: 10.1038/ngeo133).
Nenes, A., Krom, M., Mihalopoulos, N., VanCapellen, P., Shin, Z., Bougiatioti, A., Zarmpas, P., Herut, B., 2010. Atmospheric acidification of mineral aerosols: a source of bioavailable phosphorus to the oceans. Atmos. Chem. Phys. Discuss. 11, 6163–6185.
Okada, K., Heintzenberg, J., Kai, K.J., Qin, Y., 2001. Shape of atmospheric mineral particles collected in three Chinese arid-regions. Geophys. Res. Lett. 28, 3123–3126.
Okin, G., Baker, A., Tegen, I., Mahowald, N., Dentener, F., Duce, R., Galloway, J., Hunter, K., Kanakidou, M., Kubilay, N., Prospero, J., Sarin, M., Surpipith, V., Uematsu, M., Zhu, T., 2011. Impacts of atmospheric nutrient deposition on marine productivity: roles of nitrogen, phosphorus and iron. Global Biogeochem. Cycles 25 (doi: 10.1029/2010GB003858).
Okin, G., Mahowald, N., Chadwick, O., Artaxo, P., 2004. The impact of desert dust on the biogeochemistry of phosphorus in terrestrial ecosystems. Global Biogeochem. Cycles 18, GB2005, doi:2010.1029/2003GB002145.
Okin, G.S., Mladenov, N., Wang, L., Cassel, D., Caylor, K.K., Ringros, S., Macko, S.A., 2008. Spatial pattern of soil nutrients in two southern African savannas. J. Geophys. Res. 111 (doi: 10.1029/2007JG000584).
Osborne, S.R., Johnson, B.T., Haywood, J.M., Baran, A.J., Harrison, M.A.J., McConnell, C.L., 2008. Physical and optical properties of mineral dust aerosol during the Dust and Biomass-burning Experiment. J. Geophys. Res. 113, D00c03.
Painter, T., Barrett, A., Landry, C.C., Neff, J.C., Cassidy, M.P., Lawrence, C.R., McBride, K.E., Farmer, G.L., 2007. Impact of disturbed desert soils on duration of mountain snow cover. Geophys. Res. Lett. 34 (doi: 10.1029/2007GL030284).
Patadia, F., Yang, E.-S., Christopher, S., 2009. Does dust change the clear sky top of atmosphere shortwave flux over high surface reflectance regions? Geophys. Res. Lett. 36. http://dx.doi.org/10.1029/2009GL039092.
Perfect, E., Kay, B.D., 1995. Brittle-fracture of fractal cubic aggregates. Soil Sci. Soc. Am. J. 59, 969–974.
Petit, J.-R., Jouzel, J., Raynaud, D., Barkov, N.I., Barnola, J.-M., Basile, I., Bender, M., Chappellaz, J., Davisk, M., Delaygue, G., Delmotte, M., Kotlyakov, V.M., Legrand, M., Lipenkov, V.Y., Lorius, C., Pepin, L., Ritz, C., Saltzmank, E., Stievenard, M., 1999. Climate and atmospheric history of the past 420,000 years from the Vostok ice core, Antarctica. Nature 399, 429–436.
Perlwitz, J., Tegen, I., Miller, R., 2001. Interactive soil dust aerosol model in the GISS GCM 1. Sensitivity of the soil dust cycle to radiative properties of soil dust aerosols. Journal of Geophysical Research 106, 18,167–118,192.
Porter, S.C., An, Z.S., 1995. Correlation between climate events in the North Atlantic and China during the last glaciation. Nature 375, 305–308.
Prospero, J., Lamb, P., 2003. African droughts and dust transport to the Caribbean: climate change implications. Science 302, 1024–1027.
Prospero, J.M., 1996. Saharan dust transport over the North Atlantic Ocean and mediterranean: an overview. In: Guerzoni, S., Chester, R. (Eds.), The Impact of Desert Dust Across the Mediterranean. Kluwer Academic Publishers, Netherlands, pp. 133–151.
Prospero, J.M., Barrett, K., Church, T., Dentener, F., Duce, R.A., Galloway II, J.N., Moody, H.L.J., Quinn, P., 1996. Atmospheric deposition of nutrients to the North Atlantic Basin. Biogeochemistry 35, 27–73.

Prospero, J.M., Custals, L., 2012. Particle size distributions of Trade-Wind African dust measured in the air and after dispersal in water. Eos Trans. AGU, Fall Meeting (San Francisco, CA) Supplement PP21C-01.
Pye, K., 1995. The origin, nature and accumulation of loess. Quat. Sci. Rev. 14 (7–8), 653–667.
Rasch, P.J., Feichter, H., Law, K., Mahowald, N., Penner, J., Benkovitz, C., Genthon, C., Giannakopoulos, C., Kasibhatla, P., Koch, D., Levy, H., Maki, T., Prather, M., Roberts, D.L., Roelofs, G.-J., Stevenson, D., Stockwell, Z., Taguchi, S., Chipperfield, M., Baldocchi, D., McMurry, P., Barrie, L., Balkanski, Y., Chatfield, B., Jacob, D., Kritz, M., Lawrence, M., Lee, H.N., Leaitch, R., Lelieveld, J., Noone, K.J., Seinfeld, J., Stenchikov, G., Schwarz, S., Walcek, C., Williamson, D., 2000. An assessment of scavenging and deposition processes in global models: results from the WCRP Cambridge workshop of 1995. Tellus 52B, 1025–1056.
Rea, D.K., 1994. The paleoclimatic record provided by eolian deposition in the deep sea: the geologic history of wind. Rev. Geophys. 32 (2), 159–195.
Rea, D.K., Hovan, S.A., 1995. Grain size distribution and depositional processes of the mineral component of abyssal sediments: lessons from the North Pacific. Paleoceanography 10 (2), 251–258.
Reid, E., Reid, J., Meier, M., Dunlap, M., Cliff, S., Broumas, A., Perry, K., Maring, H., 2003a. Characterization of African dust transported to Puerto Rico by individual particle and size segregated bulk analysis. JGR-Atmos. 108 (doi: 10.1029/1200dJD002935).
Reid, J., Hobbs, P., Ferek, R., Blake, D., Martins, J., Dunlap, M., Liousse, C., 1998. Physical, chemical and optical properties of regional hazes dominated by smoke in Brazil. JGR 103, 32059–32080.
Reid, J.S., Jonson, H., Maring, H., Smirnov, A., Savoie, D., Cliff, S., Reid, E., Livingston, J., Meier, M., Dubovik, O., Tsay, S.-C., 2003b. Comparison of size and morphological measurements of dust particles from Africa. Journal of Geophysical Research 108, 8593, doi:1029/2002JD002485.
Reid, J.S., Reid, E.A., Walker, A., Piketh, S., Cliff, S., Al Mandoos, A., Tsay, S.C., Eck, T.F., 2008. Dynamics of southwest Asian dust particle size characteristics with implications for global dust research. J. Geophys. Res. 113.
Rosenfeld, D., Nirel, R., 1996. Seeding effectiveness-the interaction of desert dust and the southern margins of rain cloud systems in Isreal. J. Appl. Meteorol. 35, 1502–1509.
Rosenfeld, D., Rudich, Y., Lahav, R., 2001. Desert dust suppressing precipitation: a possible desertification feedback loop. Proc. Natl. Acad. Sci. USA 98, 5975–5980.
Ruth, U., Wagenbach, D., Steffensen, J. P., Bigler, M., 2003. Continuous record of microparticle concentration and size distribution in the central Greenland NGRIP ice core during the last glacial period. J. Geophys. Res., vol. 108, NO. D3, doi:10.1029/2002JD002376.
Ryder, C.L., Highwood, E.J., Lai, T.M., Sodeman, H., Masham, J.H., 2013a. Impact of atmospheric transport on the evolution of microphysical and optical properties of Saharan dust. Geophys. Res. Lett. 40.
Ryder, C.L., Highwood, E.J., Rosenberg, P.D., Trembath, J., Brooke, J.K., Bart, M., Dean, A., Crosier, J., Dorsey, J., Brindley, H., Banks, J., Marsham, J.H., McQuaid, J.B., Sodemann, H., Washington, R., 2013b. Optical properties of Saharan dust aerosol and contribution from the coarse mode as measured during the Fennec 2011 aircraft campaign. Atmos. Chem. Phys. 13, 303–325.
Schladitz, A., Muller, T., Nowak, A., Kandler, K., Lieke, K., Massling, A., Wiedensohler, A., 2011. In situ aerosol characterization at Cape Verde Part 1: particle number size distributions, hygroscopic growth and state of mixing of the marine and Saharan dust aerosol. Tellus Ser., B-Chem. Phys. Meteorol. 63, 531–548.
Schulz, M., Prospero, J., Baker, A., Dentener, F., Ickes, L., Liss, P., Mahowald, N., Nickovic, S., Perez, C., Rodriguez, S., Sarin, M., Tegen, I., Duce, R., 2012. The atmospheric transport and deposition of mineral aerosols to the ocean: implications for reseach needs. Environ. Sci. Technol. 46, 10390–10404 (doi: 10310.11021/es300073u).
Seinfeld, J.H., Pandis, S.N., 1998. Atmospheric chemistry and physics: From air pollution to climate change. John Wiley & Sons Inc., New York.
Shao, Y., 2001. A model for mineral dust emission. J. Geophys. Res. 106, 20239–20254.
Shao, Y., Ishizuka, M., Mikami, M., Leys, J.F., 2011a. Parameterization of size-resolved dust emission and validation with measurements. J. Geophys. Res. 116, D08203.
Shao, Y., Wyrwoll, K.-H., Chappel, A., Huang, J., Lin, Z., McTainsh, G., Mikami, M., Tanaka, T., Wang, X., Yoon, S., 2011b. Dust cycle: an emerging core theme in earth system science. Aeolian Res. 2, 181–204.
Shao, Y.P., 2004. Simplification of a dust emission scheme and comparison with data. J. Geophys. Res. 109.
Sholkovitz, E., Sedwick, P., Church, T., Baker, A., Powell, C., 2012. Fractional solubility of aerosol iron: synthesis of a global-scale data set. Geochim. Cosmochim. Acta 89, 173–189.
Slinn, S.A., Slinn, W.G.N., 1980. Predictions for particle deposition on natural waters. Atmos. Environ. 14, 1013–1016.
Sow, M., Alfaro, S.C., Rajot, J.L., 2011. Comparison of the size-resolved dust emission fluxes measured over a Sahelian source with the dust production model (DPM) predictions. Atmos. Chem. Phys. Discuss. 11, 11077–11107.
Sow, M., Alfaro, S.C., Rajot, J.L., Marticorena, B., 2009. Size resolved dust emission fluxes measured in Niger during 3 dust storms of the AMMA experiment. Atmos. Chem. Phys. 9, 3881–3891.
Steffensen, J.P., 1997. The size distribution of microparticles from selected segments of the Greenland Ice Core Project ice core representing different climatic periods. J. Geophys. Res. 102, C12, 26,755–26,763.
Stuut, J.B., Zabel, M., Ratmeier, V., Helmke, P., Schefuss, E., Lavik, G., Schneide, R., 2005. Provenance of present day eolian dust collected off NW Africa. J. Geophys. Res. 110, D4 (doi: 10.1029/2004JD005161).
Su, L., Toon, O., 2009. Numerical simulations of Asian dust storms using a coupled climate-aerosol microphysical model. J. Geophys. Res. 114 (doi: 10.1029/2008JD010956).
Swap, R., Garstang, M., Greco, S., Talbot, R., Kallberg, P., 1992. Saharan dust in the Amazon Basin. Tellus 44B, 133–149.
Tegen, I., Fung, I., 1994. Modeling of mineral dust in the atmosphere: Sources, transport, and optical thickness. J. Geophys. Res. 99, 22,897–822,914.
Tegen, I., Hollrig, P., Chin, M., Fung, I., Jacob, D., Penner, J., 1997. Contribution of different aerosol species to the global aerosol extinction optical thickness: Estimates from model results. J. Geophys. Res. 102, 23,895–823,915, October 827 1997.
Tegen, I., Lacis, A.A., 1996. Modeling of particle size distribution and its influence on the radiative properties of mineral dust aerosol. J. Geophys. Res. 101, 19237–19244.
Tjallingii, R., Claussen, M., Stuut, J.-B., Fohlmeister, J., Jahn, A., Bickert, T., Lamy, F., Rohl, U., 2008. Coherent high- and low-latitude control of the northwest African hydrological balance. Nat. Geosci. 1, 670–675.
Todd, M.C., Washington, R., Martins, J.V., Dubovik, O., Lizcano, G., M'Bainayel, S., Engelstaedter, S., 2007. Mineral dust emission from the Bodele Depression, northern Chad, during BoDEx 2005. J. Geophys. Res.-Atmos., 112, D06207.
van den Heever, S., Carrio, G., Cotton, W., DeMott, P., Prenni, A., 2006. Impacts of nucleating aerosols on Florida convection. Part 1: Mesoscale simulations. J. Atmos. Sci. 63, 1752–1775.
Vitousek, P., 1984. Litterfall, nutrient cycling and nutrient limitations in tropical forests. Ecology 65, 285–298.
Wang, X., Doherty, S.J., Huang, J., 2013. Black carbon and other light-absorbing impurities in snow across Northern China. J. Geophys. Res. 118 (3), 1471–1492 (doi: 10.1029/2012JD018291).
Washington, R., Todd, M.C., Engelstaedter, S., Mbainayel, S., Mitchell, F., Dust and the low-level circulation over the Bodele depression, Chad: observations from BoDEx 2005. J. Geophys. Res.-Atmos. 111, D03201.
Weidenohler, A. et al., 2012. Mobility particle size spectrometers: harmonization of technical standards and data structure to facilitate high quality long-term observations of atmospheric particle number size distributions. Atmos. Meas. Technol. 5, 657–685.
Weinzierl, B., Petzold, A., Esselborn, M., Wirth, M., Rasp, K., Kandler, K., Schutz, L., Koepke, P., Fiebig, M., 2009. Airborne measurements of dust layer properties, particle size distribution and mixing state of Saharan dust during SAMUM 2006. Tellus Ser., B-Chem. Phys. Meteorol. 61, 96–117.
Weltje, G.J., 1997. Algorithms for solving the explicit mixing problem. Math. Geol. 29 (4), 503–550.
Xiao, J., Porter, S.C., An, Z., Kumai, H., Yoshikawa, S., 1995. Grain size of quartz as an indicator of winter monsoon strength on the Loess Plateau of central China during the last 130,000 yr. Quatern. Res. 43 (1), 22–29.
Xu, J. et al., 2010. A 108.83-m ice-core record of atmospheric dust deposition at Mt. Qomolangma (Everest), Central Himalaya. Quatern. Res. 73 (1), 33–38 (doi: 10.1016/j.yqres.2009.09.005).
Yoshioka, M., Mahowald, N., Conley, A., Collins, W., Fillmore, D., Coleman, D., 2007. Impact of desert dust radiative forcing on Sahel precipitation: relative importance of dust compared to sea surface temperature variations, vegetation changes and greenhouse gas warming. J. Clim. 20, 1445–1467.
Yu, H., Chin, M., Remer, L., Kleideman, R., Bellouin, N., Bian, H., Diehl, T., 2009. Variabilty of marine aerosol fine-mode fraction and estimates of anthropogenic aerosol component over cloud-free oceans from the Moderate Resolution Imaging Spectroradiometer (MODIS). J. Geophys. Res. 114. http://dx.doi.org/10.1029/2008JD010648.
Zender, C., Bian, H., Newman, D., 2003. Mineral dust entrainment and deposition (DEAD) model: description and 1990s dust climatology. J. Geophys. Res. 108, 4416 (doi: 4410.1029/2002JD002775).
Zender, C., Miller, R., Tegen, I., 2004. Quantifying mineral dust mass budgets: terminology, constraints and current estimates. EOS 85, 509–512.
Zhang, L., Kok, J.F., Henze, D.K., Li, Q., Zhao, C., 2013. Improving simulations of fine dust surface concentrations over the Western United States by optimizing the particle size distribution. Geophys. Res. Lett. 40, 3270–3275.
Zielinski, G.A., Mershon, G.R., 1997. Paleoenvironmental implications of the insoluble microparticle record in the GISP2 (Greenland) ice core during the rapidly changing climate of the Pleistocene–Holocene transition. Geol. Soc. Am. Bull. 109 (5), 547–559.
Zhao, C., Liu, X., Leung, L.R., Johnson, B., McFarlane, S.A., Gustafson, W.I., Fast, J.D., Easter, R., 2010. The spatial distribution of mineral dust and its shortwave radiative forcing over North Africa: modeling sensitivities to dust emissions and aerosol size treatments. Atmos. Chem. Phys. 10, 8821–8838.
Zobeck, T.M., Gill, T.E., Popham, T.W., 1999. A two-parameter Weibull function to describe airborne dust particle size distributions. Earth Surf. Proc. Landforms 24, 943–955.